A Model for the Spectral Albedo of Snow. I: Pure Snow

WARREN J. WISCOMBE AND STEPHEN G. WARREN[1]

National Center for Atmospheric Research,[2] Boulder, CO 80307

(Manuscript received 15 April 1980, in revised form 28 August 1980)

ABSTRACT

We present a method for calculating the spectral albedo of snow which can be used at any wavelength in the solar spectrum and which accounts for diffusely or directly incident radiation at any zenith angle. For deep snow, the model contains only one adjustable parameter, an effective grain size, which is close to observed grain sizes. A second parameter, the liquid-equivalent depth, is required only for relatively thin snow.

In order for the model to make realistic predictions, it must account for the extreme anisotropy of scattering by snow particles. This is done by using the "delta-Eddington" approximation for multiple scattering, together with Mie theory for single scattering.

The spectral albedo from 0.3 to 5 μm wavelength is examined as a function of the effective grain size, the solar zenith angle, the snowpack thickness, and the ratio of diffuse to direct solar incidence. The decrease in albedo due to snow aging can be mimicked by reasonable increases in grain size (50–100 μm for new snow, growing to 1 mm for melting old snow).

The model agrees well with observations for wavelengths above 0.8 μm. In the visible and near-UV, on the other hand, the model may predict albedos up to 15% higher than those which are actually observed. Increased grain size alone cannot lower the model albedo sufficiently to match these observations. It is also argued that the two major effects which are neglected in the model, namely nonsphericity of snow grains and near-field scattering, cannot be responsible for the discrepancy. Insufficient snow depth and error in measured absorption coefficient are also ruled out as the explanation. The remaining hypothesis is that visible snow albedo is reduced by trace amounts of absorptive impurities (Warren and Wiscombe, 1980, Part II).

1. Introduction

Radiation is the dominant component of the surface energy balance over snow during the melting season (Langleben, 1968; Weller, 1968; Paterson, 1969). Because the shortwave albedo of snow can fall from 90 to 50% or less, depending on snow condition, it controls the rate of melting. An ability to calculate snow albedo is therefore important for predicting seasonal snowmelt and runoff rates as well as for understanding the growth and decay of snowfields, which in turn affect the global energy budget and therefore climate (Kukla and Kukla, 1974). Furthermore, it may ultimately be necessary to calculate snow albedo in climate models (which now simply specify it) if the feedback between snow albedo and climate is to be understood.

We present here a simple analytical model for snow albedo. The model is useful for the entire solar spectrum (0.3–5 μm) and is based upon the delta-Eddington approximation (Joseph *et al.*, 1976) for the bulk radiative transfer coupled with Mie calculations for the scattering by individual snow particles. The model uses no arbitrary adjustable parameters; the inputs are all observable quantities. It calculates snow albedo at any wavelength as a function of snow grain size, solar zenith angle, ratio of diffuse to direct incident solar radiation, and, for a thin snow layer, as a function of snow layer thickness and albedo of the underlying surface. We compare our model results with selected observations of these effects.

2. Previous snow albedo models

Only a small number of snow albedo models have been put forward. This undoubtedly reflects a feeling that there are not very much high-quality data against which to check such a model, that some of the data are contradictory, and that therefore at best only a crude model is justified.

The first and most widely used model is that of Dunkle and Bevans (1956). They applied the Schuster two-stream approximation to a homogeneous slab of snow on which only diffuse radiation is incident. The model contains two tunable parameters, an absorption and a scattering coefficient, and consider-

[1] Present affiliation: Cooperative Institute for Research in Environmental Sciences, University of Colorado, Boulder 80309.

[2] The National Center for Atmospheric Research is sponsored by the National Science Foundation.

0022-4928/80/122712-22$09.50

able effort has gone into finding either numbers or functional forms for these coefficients (e.g., Weller, 1969; Schwerdtfeger, 1969; Bergen, 1971, 1975; Schlatter, 1972; Grenfell, 1979). Choudhury and Chang (1979) used a two-stream theory together with the Sagan-Pollack approximation for single-scattering albedo, and a backscatter fraction (7.5%) independent of wavelength. Their dependence of albedo on particle size and wavelength was qualitatively similar to that shown by Dunkle and Bevans (1956, Fig. 3), but the actual particle size necessary to obtain a particular albedo value was as much as a factor of 4 different.

Giddings and LaChapelle (1961) put forward a diffusion or random-walk model. Their paper is considerably more sophisticated than that of Dunkle and Bevans, particularly as regards its analysis of the model's range of validity (they conclude that the model is excellent for albedos over 80% and poor for albedos under 60%); however, their model requires two tunable parameters and diffuse incidence and is not demonstrably superior to Dunkle and Bevan's model.

Barkstrom (1972) and Bohren and Barkstrom (1974) applied more modern radiative transfer techniques to the snow albedo problem. Barkstrom assumed the snowpack to be semi-infinite, grey, and isotropically scattering with only direct-beam incidence. He was then able to apply the semi-analytical solutions available for the isotropic scattering problem and show, among other things, an increase in albedo with solar zenith angle, as is found observationally.

Bohren and Barkstrom (1974) improved on this work by treating scattering from individual snow grains (assumed spherical) using geometrical optics in the limit of *small* absorption; this eliminated both the unrealistic isotropic scattering assumption and the need for tunable parameters. They then used certain scaling relations of van de Hulst to reduce the problem back to one of isotropic scattering. These authors also showed that refraction *through* snow grains, not reflection *from* them, is mainly responsible for snow albedo, a point which had not been understood by earlier authors like Dunkle and Bevans (1956) or Middleton and Mungall (1952). Berger (1979)[3] has altered Bohren and Barkstrom's treatment to calculate infrared snow emissivities by using the limit of geometric optics for *large* instead of small absorption.

In summary, it may be said that substantial progress has been made in modeling snow albedo, but that no single model is valid for all wavelengths and for an arbitrary combination of diffuse and direct incidence. None of the models, except Bohren-Barkstrom, account for the strong forward scattering from snow grains in a satisfactory fashion. A simpler yet more general analytical model would clearly be desirable.

3. Observations

a. Snow albedo

Measured snow albedos are generally high (80–90%) in the near-UV and visible (0.3–0.7 μm) but start dropping off steeply with wavelength in the near-IR between 0.8 and 1.5 μm and remain generally low for longer wavelengths. Local maxima in the albedo are found at 1.1, 1.3, 1.8 and 2.2 μm, corresponding to local minima in the absorption coefficient of ice. As snow ages with or without melting, the grain size increases and the albedo is reduced at all wavelengths.

Most field measurements have been made for spectrally averaged (all-wave) albedo, and the few spectral measurements, until very recently, have been for visible wavelengths only. Many of the latter have recently been reviewed by Mellor (1977, see our Fig. 16 which was taken from his paper). These measurements are not in agreement and in some cases are contradictory; a few are clearly wrong in their wavelength dependence. The better measurements show albedo to be fairly constant between 0.4 and 0.7 μm wavelength. Sauberer (1938), Liljequist (1956) and Holmgren (1971) all find albedo to peak between 0.4 and 0.6 μm, but disagree on the absolute value of albedo. Mellor (1977, Fig. 37) measured albedo to be erratic but generally decreasing with wavelength for $0.4 \leq \lambda \leq 0.7$ μm. Liljequist's Antarctic snow was clean, dry and fine-grained and his measurements represent a probable upper limit for snow albedo.

Whereas Holmgren and Liljequist measured albedo only at four discrete wavelengths, recent measurements with high spectral resolution have been reported for a variety of snow conditions in the Arctic Ocean by Grenfell and Maykut (1977) for $0.4 \leq \lambda \leq 1.0$ μm, and for dry snow in Antarctica by Kuhn and Siogas (1978) for $0.4 \leq \lambda \leq 1.55$ μm. Spectrally detailed measurements of bidirectional reflectance in the red and near-IR region ($0.6 \leq \lambda \leq 2.5$ μm) have been reported by O'Brien and Munis (1975),[4] and for the near-UV ($0.2 \leq \lambda \leq 0.45$ μm) by O'Brien (1977).[5]

[3] Berger, R. H., 1979: Snowpack optical properties in the infrared. CRREL Rep. 79-11, U.S. Army Cold Region Research and Engineering Lab, Hanover, NH. [NTIS AD-A071 004/6GA].

[4] O'Brien, H. W., and R. H. Munis, 1975: Red and near-infrared spectral reflectance of snow. CRREL Res. Rep. 332, 18 pp. [NTIS AD-A007 732/1GI].

[5] O'Brien, H. W., 1977: Observations of the ultraviolet spectral reflectance of snow. CRREL Rep. 77-27, 19 pp. [NTIS AD-A046 349/7GI].

Investigations have been made of the effects on snow albedo of individual parameters: solar zenith angle, cloud cover, snow age, snow depth, snow density and dust content. The albedo is found to increase as solar zenith increases, as measured on the Juneau Ice Field by Hubley (1955), on Arctic sea ice by Bryazgin and Koptev (1969), in the Rocky Mountains by Korff *et al.* (1974)[6] and on the Antarctic coast by Liljequist (1956) and Rusin (1961). Some workers, however, found the opposite trend. Havens (1964) reported highest albedos at midday, as did Kondratiev *et al.* (1964).

Cloud cover affects both the spectral distribution of irradiance and the effective zenith angle. It always causes an increase in the all-wave snow albedo. An increase of 5–10% relative to clear-sky albedo was found at Maudheim (Antarctica) by Liljequist (1956); 5–7% at the South Pole by Hanson (1960) and 11% at Mawson (Antarctica) by Weller (1968). Rusin's (1961) report is especially useful because he simultaneously measured cloud cover, solar zenith angle and all-wave albedo.

The effect of snow thickness on the albedo of a finite snowpack was reported for one wavelength ($\lambda = 0.59$ μm) by Giddings and LaChapelle (1961). They found the snow albedo reaching its asymptotic value for depths larger than a few centimeters.

The reduction of spectral albedo due to snow aging has been investigated for visible wavelengths by Holmgren (1971) and Grenfell and Maykut (1977), and for the near-IR by O'Brien and Munis (1975).[4]

b. Snow grain size

Our snow albedo model, which assumes snow grains are spheres, is sensitive to the assumed value of average grain radius. Many observations have been made of the physical size of snow crystals and how their size increases with age, and many excellent photographs of individual snow crystals and grains are available (e.g., Nakaya, 1954; LaChapelle, 1969). But for a highly nonspherical snow crystal what *is* the average radius? The optical size may not be the same as the physical size, although snow crystals tend to be large enough that the two are nearly the same in the solar spectrum. Giddings and LaChapelle (1961) speculate that the appropriate average grain radius will be proportional to V/S, the volume-to-surface ratio. This may differ from our visual estimation of size, and it means that average grain radius will increase as a grain tends toward a sphere, even if its volume remains unchanged.

Fortunately for our modeling, snow crystals quickly lose their delicate shapes after falling. They may be broken up by the wind (Liljequist, 1956). They undergo "equitemperature metamorphism" (Sommerfeld and LaChapelle, 1970; Colbeck, 1979), in which water molecules migrate from one part of a crystal to another so as to reduce its surface free energy. This energy is proportional to S/V, which is least for a sphere; therefore, the crystals tend toward a spherical shape. Furthermore, since S/V is smaller for larger spheres, the larger spheres tend to grow at the expense of the smaller ones. Water molecules migrate faster the higher the temperature, and very rapidly indeed in snow at the melting point. Sooner or later, the snow grains become not only rounded but of fairly uniform size.

Grain size may vary by several factors with depth (e.g., Stephenson, 1967), but generally it is only the topmost 10–20 cm of snow which determine albedo, and in this region the grain size generally varies by less than 50%.

Snow grain metamorphism in Antarctica has been observed (Stephenson, 1967; Gow, 1969) to follow the same relationship as grain growth by sintering in metals and ceramics, *viz.*,

$$D^2 - D_0^2 = \alpha t e^{-\beta/T},$$

where D is grain diameter, t is time, T is Kelvin temperature, and α and β are constants. This relationship offers the hope that our model will eventually be able to predict snow albedo as a function of age and temperature, rather than grain radius.

An examination of a wide variety of references (Nakaya, 1954; Liljequist, 1956; Arai, 1966; Colbeck, 1975; Gow, 1969; Hobbs, 1974; LaChapelle, 1969; Mellor, 1977; O'Brien and Munis, 1975,[4] Sommerfeld and LaChapelle, 1970; Stephenson, 1967) suggests average grain radii in the range 20–100 μm for new snow, 100–300 μm for fine-grained older snow, and 1.0–1.5 mm for old snow near the melting point. Therefore, in many of our examples, we shall use average grain radii of 50, 200 and 1000 μm as representative of the range which exists in nature.

4. Snow albedo model

Our approach was to design the simplest and most straightforward model possible, which would still be sophisticated enough to account for

- The wide variability in ice absorption with wavelength.
- The extremely forward-directed scattering from snow grains.
- An arbitrary mix of diffuse and direct radiation striking the snow surface.

[6] Korff, H. C., J. Gailiun and T. Vonder Haar, 1974: Radiation measurements over a snowfield at an elevated site. Atmos. Sci. Pap. No. 221, Colorado State University, [NTIS N74-31878/3GI].

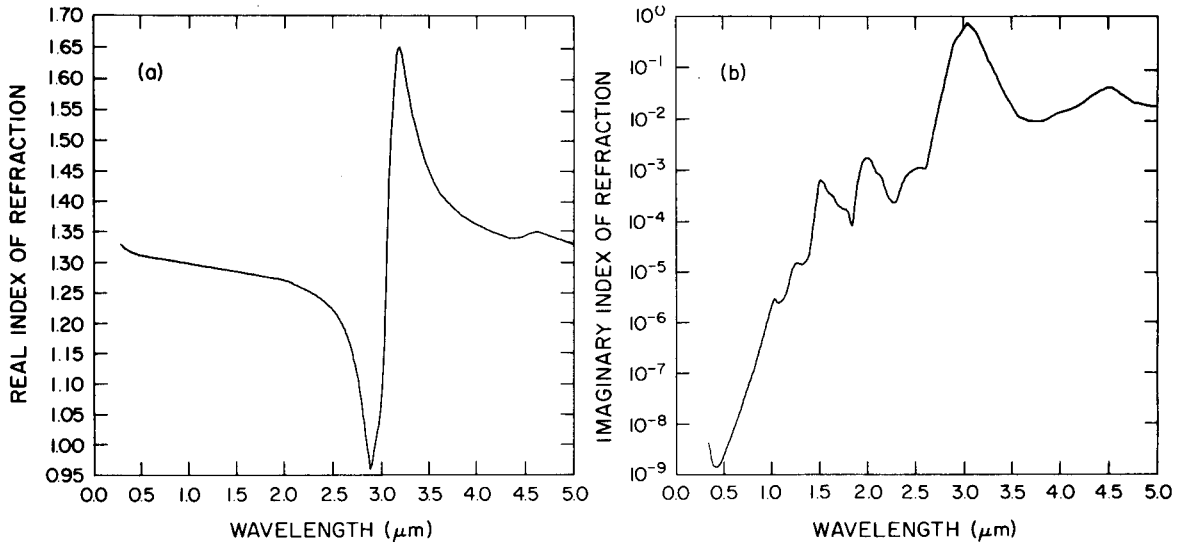

FIG. 1. Real and imaginary refractive index of ice at −7°C, as a function of wavelength.

Previous models have been deficient in one or more of these areas (see Section 2). Our model depends on directly observable variables, rather than empirical or tunable parameters. These variables are

$m(\lambda)$	complex refractive index of ice $[=m_{re}(\lambda) - im_{im}(\lambda)]$
λ	wavelength
r	mean snow grain radius
μ_0	cosine of solar zenith angle θ_0
R	ratio of diffuse incident flux to total (direct and diffuse) incident flux
L	equivalent depth of liquid water in snowpack (g cm^{-2})
A	albedo of surface beneath snow.

The last two variables are only used if the snow is so thin that the underlying surface "shows through." L is obtained as the product ρd, where ρ is the snow density (g cm^{-3}) and d the snow thickness (cm). The ice volume absorption coefficient is

$$\beta_{abs} = 4\pi\lambda^{-1}m_{im}(\lambda)$$

and assumes the same units as λ^{-1}. This relation has been used to deduce m_{im} from measured values of β_{abs} in some spectral regions.

a. Ice refractive index

The careful measurements of ice refractive index at −7°C by Schaaf and Williams (1973) are used for the real refractive index $m_{re}(\lambda)$ when $\lambda \geq 2$ μm and for the imaginary index $m_{im}(\lambda)$, $\lambda \geq 2.77$ μm. For other wavelengths we employed a congeries of sources to be described below. Our deduced refractive index values are plotted in Fig. 1 from $\lambda = 0.30$ to 5 μm. (Radiation at wavelengths < 0.30 μm does not reach the surface.) A tabular rendition of Fig. 1 is available from the authors.

Linear interpolation was used to obtain values of $m_{re}(\lambda)$ at wavelengths between those where measurements were available. The actual procedures used to obtain $m_{re}(\lambda)$ in the various wavelength intervals were as follows:

1) 0.3–0.4 μm: Linear extrapolation from Hobbs' (1974) Table 3.1.

2) 0.4–0.55 μm: Hobbs' (1974) Table 3.1 gives two values of m_{re}, one for the ordinary ray (m_{re}^0) and one for the extraordinary ray (m_{re}^e), which differ only slightly because ice birefringence is small; these are weighted by the fraction of energy going into each ray and averaged, $m_{re} = \frac{2}{3}m_{re}^0 + \frac{1}{3}m_{re}^e$.

3) 0.55–2 μm: Linear interpolation between Hobbs' value at 0.55 μm and Schaaf and Williams' value at 2.0 μm, which differ by only 0.04 so that the error incurred by this long interpolation should be of little consequence. Earlier measurements by Bode (1909) and Kislovskii (1959), as reworked by Irvine and Pollack (1968), disagree with Schaaf and Williams in the region where they overlap, and so we reject them. (Irvine and Pollack admit that their sources are unreliable for $1 \leq \lambda \leq 3$ μm.)

For the $m_{im}(\lambda)$ values in Fig. 1, we performed logarithmic interpolation (assuming $\ln m_{im}$ to be linear in λ) between available measurements. Measurements in the region 1.40–2.65 μm were corrected to −7°C using the temperature dependences of Irvine and Pollack [1968, Eq. (1) and Table 3]. (The temperature dependence is quite small.) Our detailed procedures for the various wavelength intervals were as follows:

4) 0.3–0.313 μm: Logarithmic extrapolation from

Sauberer's (1950) value at 0.313 μm, using the trend of the $m_{im}(\lambda)$ curve for liquid water (Irvine and Pollack, 1968, Fig. 1a) as a guide.

5) 0.313–0.80 μm: Sauberer's (1950) measurements of light transmission through 15–50 cm thick plane-shaven blocks of clean bubble-free lake ice. His assumption of a 4% reflection loss at the plane interfaces is a modest overestimate of the calculated Fresnel reflectance at normal incidence, but the corrected absorption coefficients would be *at most* a factor of 1.4 greater and this turned out to have a negligible effect on our calculated snow albedos at these wavelengths. Sauberer noted that his absorption coefficients were roughly an order of magnitude smaller than those of Kalitin (1936), who also used lake ice. The measurements of ice absorption in this spectral region are more uncertain than in almost any other, because of the long path lengths of pure ice required and because of possible scattering from microbubbles. Comparison with the more carefully measured curves for water (Hale and Querry, 1973; Palmer and Williams, 1974) reveal much more structure around 0.6, 0.75 and 0.97 μm than Sauberer found in the ice curves, and because of the structural similarities between the water and ice curves in other spectral regions, one strongly suspects that the ice curves have just not been measured well enough from 0.3 to 1 μm.

6) 0.80–0.95 μm: Logarithmic interpolation from Sauberer's (1950) "visible series" measurement at 0.80 μm to Luck's (1963) measurement at 0.95 μm. The Luck value is the one favored by Irvine and Pollack (1968), who quote no values of $m_{im}(\lambda)$ below $\lambda = 0.95$ μm. Sauberer made measurements within this spectral region but cautioned that the values were order-of-magnitude only. They deviate typically by 20% from Luck's values for 0.95–1.1 μm and even more than that from Sauberer's own "visible series" value at 0.8 μm, so we have ignored them. While Lyons and Stoiber (1959) give an excellent critical review of previous measurements, we chose not to use their measurements for this region because they are lower than Luck's by a factor of 2 or so.

7) 0.95–2.65 μm: Based on Irvine and Pollack's (1968) recommendations, we used Luck (1963) for 0.95–1.30 μm, Ockman (1958) for 1.40 μm and 1.9–2.1 μm, and Reding (1951) for 1.45–1.85 μm and 2.15–2.65 μm. The largest uncertainty is near 1.85 μm, where neither Reding's nor Ockman's values are reliable because transmissions through their ice samples were close to 100%. Reding's sample thickness was also poorly determined. Use of his value at 1.85 μm leads to poor agreement between our model and observed snow albedo just near that wavelength (Ockman's value gives an equal disagreement in the opposite direction.)

8) 2.65–2.77 μm: Logarithmic interpolation between Schaaf and Williams' value at 2.77 μm and Reding's value at 2.65 μm.

b. Scattering by individual snow grains

We have assumed the individual snow grains scatter like spheres in each other's far fields (we discuss the relaxation of the far-field assumption in Section 7). In reality, of course, snow grains are not exactly spherical, but there are still several compelling reasons for assuming sphericity (reviewed by Mugnai and Wiscombe, 1980). The possible effects of nonsphericity on snow albedo are discussed in Section 7b.

The formulas for scattering by spheres are reviewed by van de Hulst (1957). They require as input the dimensionless size parameter $x = 2\pi r/\lambda$ and the complex refractive index $m(\lambda)$. We require as output the three quantities:

$\sigma_{ext} = \pi r^2 Q_{ext}$ = extinction cross section,

$\tilde{\omega} = \dfrac{\sigma_{sca}}{\sigma_{ext}}$ = single-scatter albedo (ratio of scattering to extinction cross-section),

g = asymmetry factor (mean value of $\cos\theta$, where θ is scattering angle).

The first quantity σ_{ext} is required only when the snow layer is *not* optically semi-infinite; Q_{ext} is the dimensionless "extinction efficiency." Both $\tilde{\omega}$ and g are dimensionless with ranges $0 \leq \tilde{\omega} \leq 1$ and $-1 \leq g \leq 1$. $g = 0$ corresponds to isotropic scattering and $g = 1$ to completely forward-directed scattering. Plots of the variations of Q_{ext}, $\tilde{\omega}$ and g with x and with $m(\lambda)$ may be found in the review paper of Hansen and Travis (1974).

All three quantities, Q_{ext}, $\tilde{\omega}$ and g, approach definite geometric-optics limits as $x \to \infty$ (e.g., $Q_{ext} \to 2$), albeit at different rates. But even though $x > 50$ and more typically $x \gg 50$ for snow grains in the solar spectrum, we found that the actual geometric-optics limiting values were *not* always accurate enough, especially in the near infrared and for the smaller grain sizes. Therefore, we calculated the exact spherical Mie results using the fast algorithms of Wiscombe (1979, 1980). However, Mie quantities as a function of x contain a quasi-oscillatory "ripple" which causes erratic fluctuations in the spectral albedo curves. Such fluctuations are unrealistic because there is always a sufficient range of grain sizes in snow to eliminate them. We have eliminated the ripple by averaging over a range of sizes which is small relative to the mean grain size.

Figs. 2–4 show our calculated values of Q_{ext}, $1 - \tilde{\omega}$, and g as a function of wavelength across the solar spectrum (0.3–5.0 μm). Q_{ext} and g are rela-

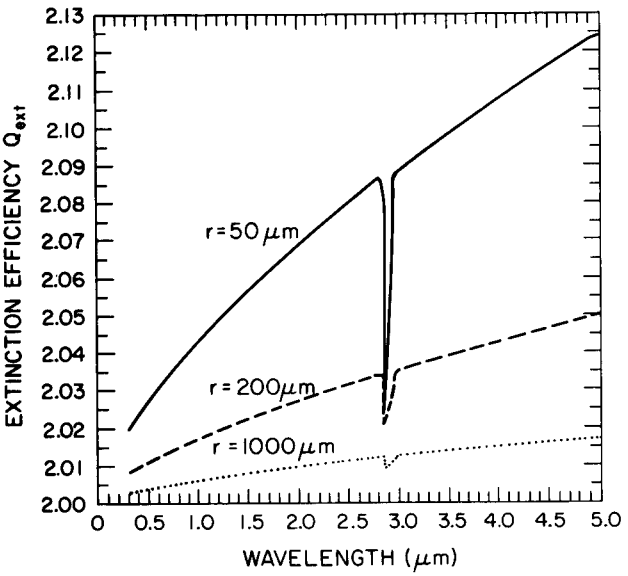

FIG. 2. Extinction efficiency (Q_{ext}) for ice spheres of various radii, as a function of wavelength.

tively weak functions of wavelength compared to $1 - \tilde{\omega}$, and so we shall find later that the spectral variation of snow albedo is caused almost exclusively by $1 - \tilde{\omega}$.

In Fig. 2 we see that the larger the grain radius, the closer Q_{ext} is to its geometric-optics value of 2. It departs increasingly from 2 as wavelength increases, although even for 50 μm grains at $\lambda = 5$ μm the departure is only 6%. The sharp dips at the 3 μm absorption edge, where $m_{re} \to 1$, occur because the Fresnel reflectances at the surface of the sphere nearly vanish there, virtually eliminating the reflection contribution to Q_{ext}.

The coalbedo $1 - \tilde{\omega}$ (Fig. 3) rises fairly monotonically from values in the neighborhood of 10^{-5} in the visible to values between 0.1 and 0.5 at $\lambda = 1.5$ μm. The upper limit is ~0.5 rather than 1.0, for reasons explained in Hansen and Travis (1974); as a consequence there is always *some* scattering, and the snow albedo will never strictly go to zero, although it does dip to values between 0.1 and 1% in the regions of strongest absorption. Beyond $\lambda = 1.5$ μm the coalbedo is plotted on a linear scale and can be seen to undergo large variations as a consequence of the various ice absorption bands in Fig. 1. Near $\lambda = 3$ μm, where ice absorption is maximal ($m_{im} \lesssim 1$), one begins to enter the "mirror-reflection" regime typical of highly-conducting metals, and here $1 - \tilde{\omega}$ actually *decreases* as m_{im} increases. Later we shall see that this produces a seemingly paradoxical local *maximum* in snow albedo just past $\lambda = 3$ μm.

The asymmetry factor g (Fig. 4) assumes values in the fairly narrow range 0.88 to 1.0, with smaller and fairly uniform values across the visible, and larger and more variable values across the near infrared. It rises to ~0.997 at the 3 μm absorption edge, which is due to the aforementioned vanishing of the reflection contribution to scattering (leaving only diffraction). Even though the values of g are rather restricted in range, the snow albedo is distinctly affected by it since mean photon path lengths in the snow are sensitive functions of g, being longer, the larger g is.

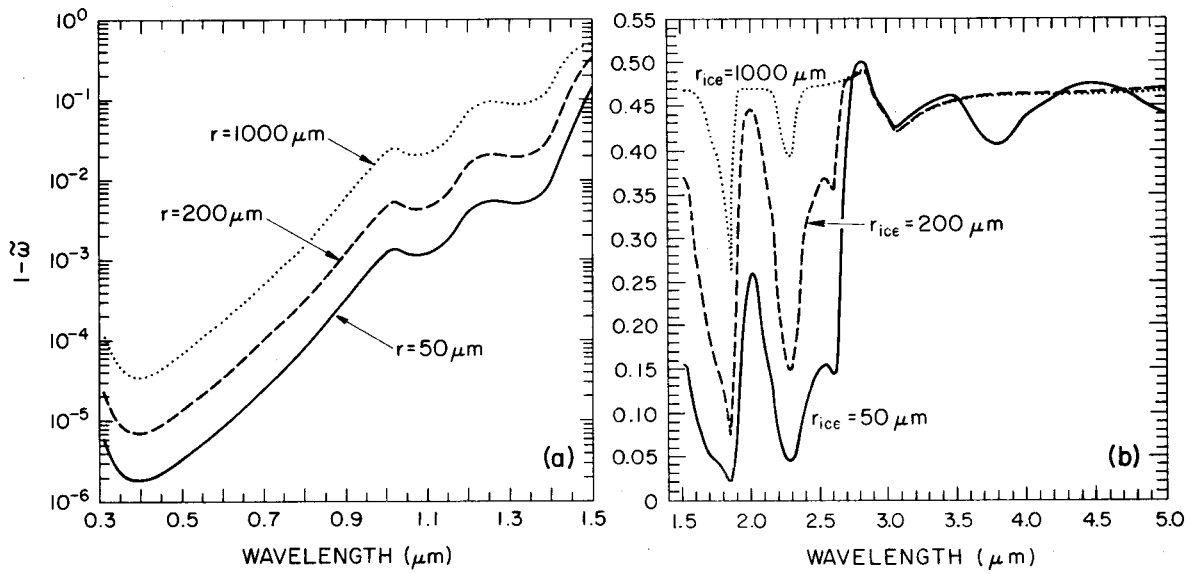

FIG. 3. Single-scattering coalbedo ($1 - \tilde{\omega}$) for ice spheres of various radii, as a function of wavelength.

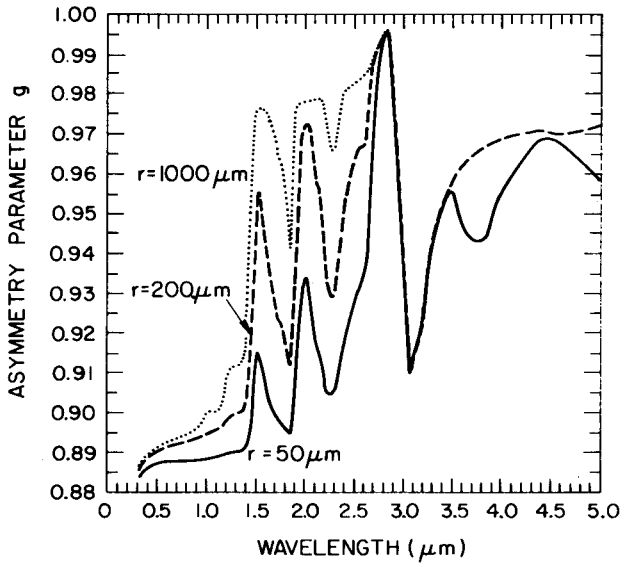

FIG. 4. Asymmetry factor g for ice spheres of various radii, as a function of wavelength.

The sharp spikes near $\lambda = 1.85$ μm in both the g and $1 - \tilde{\omega}$ plots are produced by values of ice imaginary index which, as noted previously, we consider unreliable.

c. Multiple scattering in the snowpack

The radiative transfer model which best fulfilled the stipulations at the beginning of this section was, we felt, the delta-Eddington approximation (Joseph *et al.*, 1976). It was designed specifically to handle strongly forward-directed scattering (i.e., $0.6 \leq g < 1$) such as we have in the case of a snowpack. As further demonstrated by Wiscombe and Joseph (1977), it is a good approximation over the complete ranges of $\tilde{\omega}$, g, and snow optical depth

$$\tau_0 = N\sigma_{\text{ext}}d = \frac{L\sigma_{\text{ext}}}{\frac{4}{3}\pi r^3\rho_{\text{ice}}} = \frac{3LQ_{\text{ext}}}{4r\rho_{\text{ice}}}, \qquad (1)$$

where N is number density of snow grains and ρ_{ice} is the density of pure ice (0.917 g cm^{-3}). The delta-Eddington approximation is capable of accounting for direct-beam as well as diffuse incidence on the snowpack, or any arbitrary mixture of the two. Thus we are able to eliminate a number of the restrictions inherent in some of the earlier multiple-scattering models for snow (Section 2).

The delta-Eddington approximation begins by transforming the three fundamental variables τ_0, $\tilde{\omega}$, and g as follows:

$$g^* = \frac{g}{1+g}, \qquad (2a)$$

$$\tilde{\omega}^* = \frac{(1-g^2)\tilde{\omega}}{1-g^2\tilde{\omega}}, \qquad (2b)$$

$$\tau_0^* = (1-\tilde{\omega}g^2)\tau_0. \qquad (2c)$$

Then the ordinary Eddington approximation is applied to a layer described by τ_0^*, $\tilde{\omega}^*$ and g^*. Note that this new fictitious layer is much less forward scattering ($g^* < \frac{1}{2}$), more absorptive ($\tilde{\omega}^* < \tilde{\omega}$), but less optically thick ($\tau_0^* < \tau_0$) in just the right proportion that the absorption part of the layer optical depth is unaltered. Only the scattering optical depth is reduced.

Note that when $\tilde{\omega}$ is near unity (in the 0.3–1.0 μm wavelength region for snow), one has $\tau_0^* \approx 0.2\tau_0$, which means that it takes a five times larger depth of snow to be effectively semi-infinite at these wavelengths than it would if snow were an isotropic scatterer.

Let us first assume that only a direct beam is incident at zenith angle $\theta_0 = \cos^{-1}\mu_0$. Assume further a diffusely-reflecting surface of albedo A below the snowpack. The delta-Eddington formula for the snowpack albedo a_s in this case is

$$Qa_s(\mu_0) = 2\left[P(1-\gamma+\tilde{\omega}^*b^*) + \tilde{\omega}^*(1+b^*)\frac{\gamma\xi\mu_0 - P}{1-\xi^2\mu_0^2}\right] \times \exp(-\tau_0^*/\mu_0) - \tilde{\omega}^*b^*(Q^+ - Q^-) + \tilde{\omega}^*(1+b^*)\left(\frac{Q^+}{1+\xi\mu_0} - \frac{Q^-}{1-\xi\mu_0}\right), \qquad (3)$$

where

$$a^* = 1 - \tilde{\omega}^*g^*,$$
$$b^* = g^*/a^*,$$
$$\xi = [3a^*(1-\tilde{\omega}^*)]^{1/2},$$
$$P = 2\xi/(3a^*),$$
$$\gamma = (1-A)/(1+A),$$
$$Q^\pm = (\gamma \pm P)\exp(\pm\xi\tau_0^*),$$
$$Q = (1+P)Q^+ - (1-P)Q^-.$$

The formula for $a_s(\mu_0)$ has been written in order to display the entire μ_0-dependence explicitly, with a view to later integration over μ_0. For $\tilde{\omega}^* = 1$, there is a removable singularity (of the form 0/0); but for a snowpack the nonabsorbing $\tilde{\omega}^* = 1$ case never occurs, otherwise albedos of 100% would be observed. And the formula (3) is well-behaved computationally even for $\tilde{\omega}^*$ very near 1, because ξ (and therefore P) go to zero only as $(1-\tilde{\omega}^*)^{1/2}$, which is a much larger quantity than $(1-\tilde{\omega}^*)$ itself. The formula has another removable singularity at $\mu_0 = 1/\xi$ if $\xi \geq 1$, which can only occur if ω^*

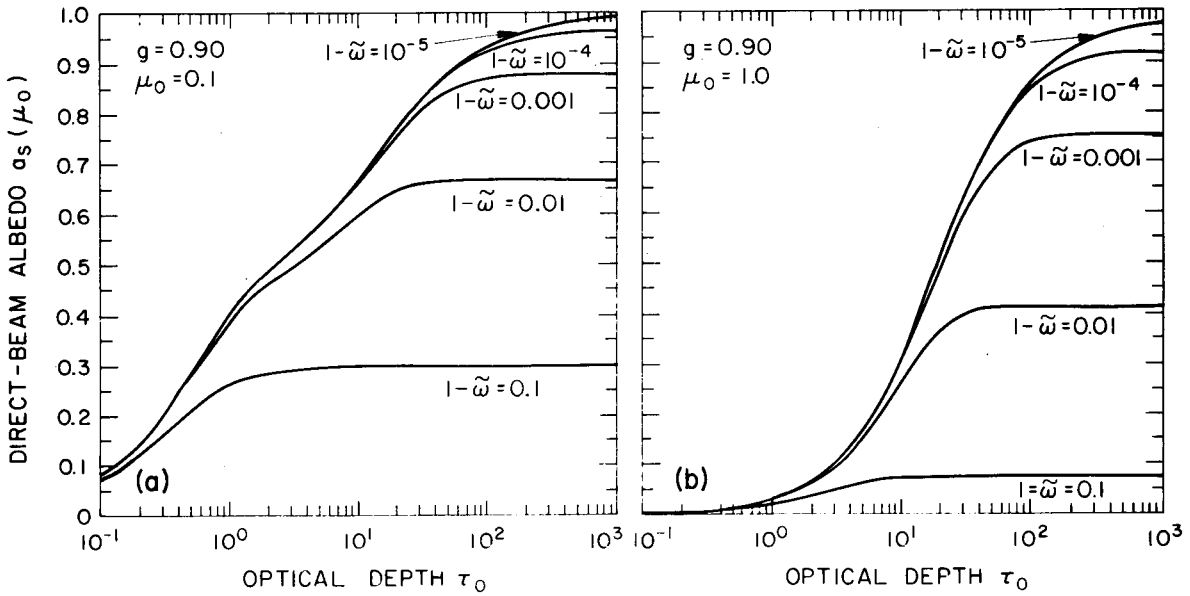

FIG. 5. Direct-beam albedo $a_s^\infty(\mu_0)$ versus snowpack optical thickness τ_0 for various values of single-scattering coalbedo $(1 - \tilde{\omega})$.

$< \frac{2}{3}$; this singularity requires special attention when integrating $a_s(\mu_0)$ over μ_0 analytically.

Fig. 5 shows $a_s(\mu_0)$ as a function of optical depth τ_0 of the snowpack for a black underlying surface ($A = 0$). A typical value $g = 0.9$ is taken for the asymmetry factor, and extreme cases of near-grazing incidence ($\mu_0 = 0.1$) and normal incidence ($\mu_0 = 1.0$) are shown. The approach of $a_s(\mu_0)$ to its semi-infinite ($\tau_0 \to \infty$) value

$$a_s^\infty(\mu_0) = \frac{\tilde{\omega}^*}{1+P}\,\frac{1-b^*\xi\mu_0}{1+\xi\mu_0}\,. \qquad (4)$$

is slower and slower, the smaller $1 - \tilde{\omega}$ is. $\tau_0 = 7$ is effectively semi-infinite for $1 - \tilde{\omega} = 0.1$, while for $1 - \tilde{\omega} = 10^{-5}$ the semi-infinite limit has barely been attained at $\tau_0 = 1000$. Thus Fig. 3 and Fig. 5 together show that infinitesimal depths of snow are effectively semi-infinite at near infrared wavelengths, while depths at least two orders of magnitude larger are required at visible wavelengths (this point is discussed further in Section 5e). By comparing the two parts of Fig. 5, one can see that the sun angle (μ_0) effect is strongest at the smaller optical depths and becomes weaker as optical depth increases.

The sun angle dependence is much weaker in the visible (small $1 - \tilde{\omega}$) cases than in the near infrared cases, which can be seen in Fig. 6 where $a_s^\infty(\mu_0)$ is plotted versus μ_0 for $g = 0.90$. The μ_0 dependence is so weak for the visible cases ($1 - \tilde{\omega} = 10^{-4}, 10^{-5}$) that it would be difficult to detect experimentally. Furthermore, $a_s^\infty(\mu_0)$ is almost perfectly linear in μ_0 for $1 - \tilde{\omega}$ up to 10^{-3}, and fairly linear even up to $1 - \tilde{\omega} = 0.1$.

Observations of the sun-angle dependence of snow albedo by Hubley (1955), Liljequist (1956), Rusin (1961), Bryazgin and Koptev (1969), and Korff

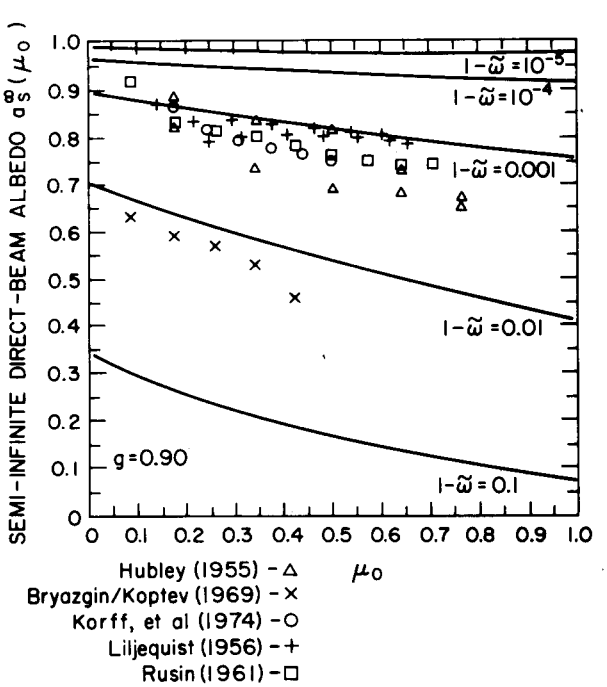

FIG. 6. Semi-infinite direct beam albedo $a_s^\infty(\mu_0)$ versus cosine of direct-beam zenith angle μ_0, for several values of single-scattering coalbedo $(1 - \tilde{\omega})$.

et al. (1974)[6] are also plotted on Fig. 6. The Bryazgin/Koptev measurements refer to a 0.6–1.2 μm wavelength interval, and are best fitted by the $1 - \tilde{\omega} = 0.01$ curve; from Fig. 3, however, it appears that $1 - \tilde{\omega} = 0.001$ is a more appropriate mean value for this wavelength interval. The reason for this discrepancy is not clear, but may be due to the presence of impurities (see Part II). The remaining measurements refer to the whole solar spectrum and are very roughly fitted by the $1 - \tilde{\omega} = 0.001$ curve since the mean value of g (see Fig. 4) is between 0.9 and 0.95. All except the measurements of Hubley tend to be in rough agreement with our predicted μ_0-dependence; but as Hubley himself notes, there is considerable disagreement in the literature over the nature of this dependence, and his measurements seem to exhibit a stronger μ_0 dependence than subsequent investigators have found.

Under overcast skies the incident flux will be diffuse rather than direct. It is possible to derive a simple formula for the albedo in this case by applying a diffuse-flux upper boundary condition to the delta-Eddington equations, but Wiscombe (1977) has shown that this formula sometimes yields negative albedos, *especially* for the semi-infinite case of most interest for snow. Therefore, we prefer to get the diffuse albedo a_d by assuming isotropically incident radiation and integrating the direct-beam albedo (3) over all angles of incidence:

$$a_d = 2\int_0^1 \mu_0 a_s(\mu_0)\,d\mu_0. \tag{5}$$

This will always be positive because it can be shown that $a_s(\mu_0)$ is always positive. Putting (3) into (5) and performing some rather lengthy manipulations leads to

$$Qa_d = 2P\left[(1 - \gamma + \tilde{\omega}^* b^*)(1 - \tau_0^*) - \frac{\gamma\tilde{\omega}^*(1 + b^*)}{1 - \tilde{\omega}^*}\right]\exp(-\tau_0^*) - 2P\left[\tilde{\omega}^*(1 + b^*)\left(\frac{2}{\xi^2} + \frac{\gamma\tau_0^*}{1 - \tilde{\omega}^*}\right)\right.$$
$$\left. + (1 - \gamma + \tilde{\omega}^* b^*)\tau_0^{*2}\right]\mathrm{Ei}(-\tau_0^*) + \frac{2\tilde{\omega}^*(1 + b^*)}{\xi^2}\left[Q^+\{\mathrm{Ei}[-(1 + \xi)\tau_0^*] + \xi - \ln(1 + \xi)\}\right.$$
$$\left. - Q^-\{\mathrm{Ei}[-(1 - \xi)\tau_0^*] - \xi - \ln|1 - \xi|\}\right] - \tilde{\omega}^* b^*(Q^+ - Q^-), \tag{6}$$

where Ei is the exponential integral:

$$\mathrm{Ei}(x) = \begin{cases} -\displaystyle\int_{-x}^{\infty} e^{-t}t^{-1}dt, & x < 0 \\ -\displaystyle\lim_{\epsilon\to 0^+}\left[\int_{-x}^{-\epsilon} + \int_{\epsilon}^{\infty}\right]e^{-t}t^{-1}dt, & x > 0. \end{cases}$$

The upper definition of $\mathrm{Ei}(x)$ is equivalent to $-E_1(-x)$ (cf. Abramowitz and Stegun, 1965, p. 228) and the lower definition is the Cauchy principal value of the same integral. This same Cauchy principal value also is used to evaluate the integral leading to the $\ln|1 - \xi|$ term when $\xi > 1$. Note that the expression in braces containing $\ln|1 - \xi|$ is finite as $\xi \to 1$ even though $\ln|1 - \xi|$ blows up in that limit.

One finds diffuse albedo equal to direct albedo ($a_d = a_s$) at any optical depth for $\mu_0 = 0.6$–0.7, corresponding to solar elevations between 37 and 44°. This conclusion is quite insensitive to asymmetry factor in the expected range ($g = 0.8$–1.0) for snow. Thus the formation of cloud cover over snow should raise its spectral albedo for solar elevations exceeding ~40° and lower it for solar elevations below 40°.

In the semi-infinite limit the diffuse albedo becomes

$$a_d^\infty = \frac{2\tilde{\omega}^*}{1 + P}\left\{\frac{1 + b^*}{\xi^2}[\xi - \ln(1 + \xi)] - b^*/2\right\}. \tag{7}$$

In Fig. 7, a_d^∞ is plotted versus $1 - \tilde{\omega}$ for several values of g relevant to snow. One sees that for the small values of $1 - \tilde{\omega}$ typical of the visible, a_d^∞ is only weakly dependent on the asymmetry factor. For the larger values of $1 - \tilde{\omega}$ typical of the near infrared, a_d^∞ exhibits considerably more sensitivity to g.

For a combination of direct and diffuse incident radiation with a diffuse fraction R, the net albedo predicted by the model is

$$a_{\mathrm{net}} = Ra_d + (1 - R)a_s(\mu_0). \tag{8}$$

5. Spectral albedo calculations for pure snow

The parameters which influence the albedo are grain size, solar zenith angle, ratio of diffuse to direct incident flux and snow layer thickness. We examine the effect of each of these parameters in turn, keeping the other parameters fixed at "standard" values of semi-infinite snow depth, 100 μm grain radius, and direct solar radiation at 60° zenith angle incident on the snow surface. These standard conditions would be characteristic of a new-fallen

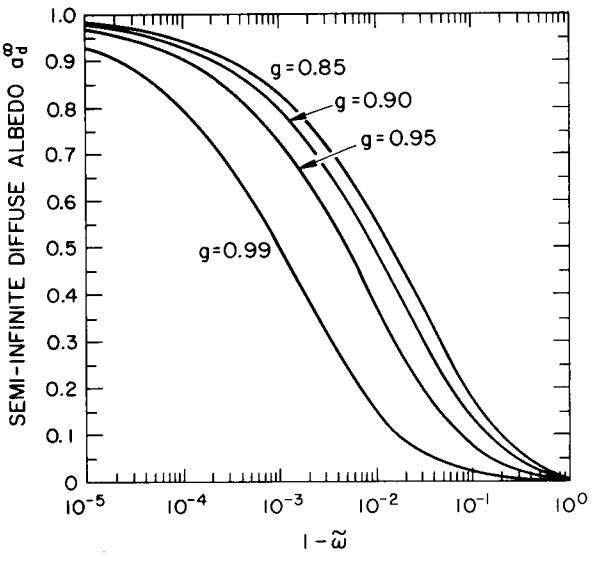

FIG. 7. Semi-infinite diffuse albedo a_d^s versus single-scattering coalbedo $1 - \tilde{\omega}$ for several values of asymmetry factor g.

snow pack deeper than 30 cm under clear skies, either in winter at midlatitudes or in spring and summer at high latitudes. We also investigate the sensitivity of our results to uncertainty in the reported absorption coefficient of ice.

It should be borne in mind that the spectrally integrated albedo is weighted by the solar spectral flux reaching the surface, so that failure to calculate correct albedo at short wavelengths is more serious than at longer wavelengths. The albedo is very low, 5% or less, for $\lambda \geq 2.8$ μm, so this spectral region will contribute practically nothing to the spectrally integrated snow albedo.

a. Dependence on grain size (or age)

Fig. 8 shows the spectral albedo for several values of the grain radius. The plotting increment is 0.01 μm from 0.3 to 2.8 μm, and beyond that just the wavelengths at which Schaaf and Williams (1973) measured ice imaginary index are used. Fig. 8b is plotted from 2.8 to 12 μm wavelength on an expanded vertical scale to show the small but nonzero albedo values which obtain in that range. Since grain size generally increases as the snow ages, it is clear from this figure that the albedo falls at all wavelengths as the grain radius *or* the age increases. This is due to the fact that larger grains are both more absorptive and more forward scattering. But for $\lambda < 2.5$ μm the fall in albedo is primarily due to the decrease in $\tilde{\omega}$ (see Fig. 3); the increase in asymmetry factor (Fig. 4) is comparatively small. At $\lambda = 1.3$ μm, for example, $g = 0.89$ for $r = 50$ μm and increases only to $g = 0.91$ for $r = 1000$ μm, whereas $\tilde{\omega}$ decreases from 0.995 to 0.91. (This is reminiscent of Hansen and Pollack's (1970) finding that "for wavelengths less than 2.5 μm the reflectivity of thick clouds depends primarily on the single-scattering albedo.")

The largest effect of grain size is seen in the near infrared, where the albedo may fall by a factor of 2 or more between $r = 50$ μm and $r = 1000$ μm. By comparison, the reductions of albedo in the visible are small, never exceeding 10–15%. Thus the fall in spectrally integrated albedo with age, which frequently has been observed in the field, is primarily due to the near infrared. This agrees with satellite observations by Strong *et al.* (1971), who saw little change in the visible channel between dry snow and melting snow, but a dramatic drop in the near-IR reflectance due to melting.

There are peaks in albedo near $\lambda = 0.4$, 1.1, 1.3, 1.85 and 2.3 μm which correspond to the minima in the absorption coefficient (Fig. 1). Unlike the other peaks, the main one at $\lambda = 0.4$ μm becomes more pronounced as the grain size increases.[7] There is also a peak at $\lambda = 3.1$ μm, which corresponds to a *maximum* in ice absorption. In this case absorption is so large that the grains have augmented backreflection (like polished metal spheres). We are not aware of any experimental confirmation of this rather peculiar peak.

At $\lambda = 2.0$ μm and 2.8 μm the albedo reaches minimum values of 0.007 and 0.001 beginning at grain radii of 500 and 100 μm, respectively; further increase in size does not further decrease the albedo below these residuals. Between $\lambda = 3.5$ μm and $\lambda = 9$ μm the residual albedo is 0.01, and it is attained for all grains larger than $r = 100$ μm. These residuals are due to the fact that $\tilde{\omega}$ has a lower limit of about 0.5 as noted in Section 4b.

Beyond $\lambda = 5$ μm, the albedo results (Fig. 4b) are really only of use to calculate the directional emissivity, which follows immediately from

$$\epsilon_s(\mu) = 1 - a_s(\mu) \tag{9}$$

as a consequence of Kirchhoff's law (Siegel and Howell, 1972). Clearly, our model is predicting emissivities of ~99% in this case, in agreement with observations of Griggs (1968), although there is a significant zenith angle dependence which we shall

[7] Some investigators find the main peak in spectral albedo to be at larger wavelengths than 0.4 μm. In our calculation, this peak corresponds to the minimum in the measured absorption coefficient of ice. Assuming that our source (Sauberer, 1950) used an 18 cm block of ice, his measured transmittances were 99.3, 99.1 and 98.5% at $\lambda = 0.40$, 0.45 and 0.50 μm, respectively. A very slight error in Sauberer's measurements could shift the calculated albedo maximum. But the deep blue color in glacial crevasses indicates the peak cannot be at a wavelength far from 0.4 μm. The observations of peaks at larger wavelengths are probably due to dust in the snow (see Fig. 5 of Part II).

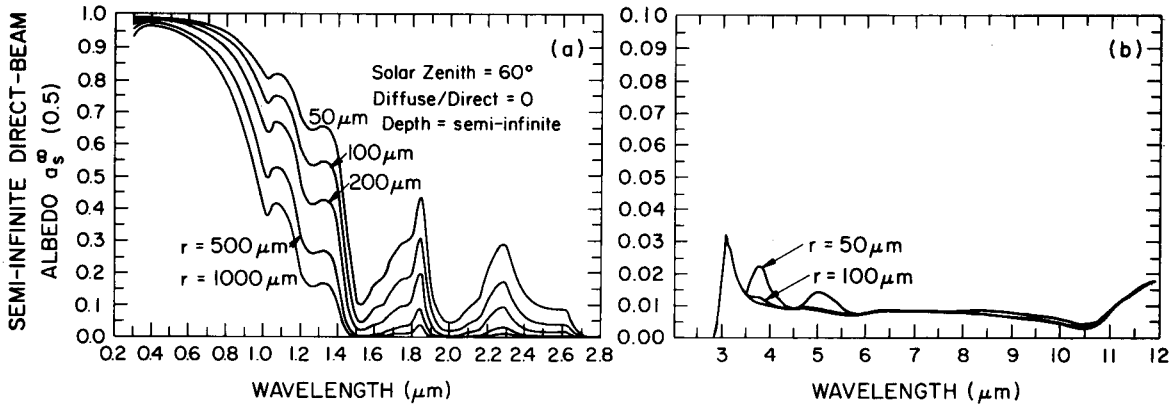

FIG. 8. Semi-infinite direct beam albedo $a_s^\infty(0.5)$ as a function of wavelength for various grain radii.

see later. The emissivity exhibits very little dependence on grain size.

Bohren and Barkstrom (1974), by assuming a single-scattering albedo close to unity (valid for the visible part of the spectrum), derived a simplified relation between semi-infinite diffuse albedo and grain size [their Eq. (42)]

$$1 - a_d^\infty \propto r^{1/2}. \tag{10}$$

This square-root dependence on grain size was also found by Giddings and LaChapelle (1961, their Eq. 21). To determine the extent of its validity, we have plotted a_d^∞ in Fig. 9 versus the square root of the grain radius for several wavelengths. We see that the relation (10) holds for the visible wavelengths 0.4 and 0.8 μm but not for longer wavelengths. This breakdown in (10) occurs whenever $\tilde{\omega}$ drops below 0.99, i.e., beyond about $\lambda = 0.9\ \mu$m.

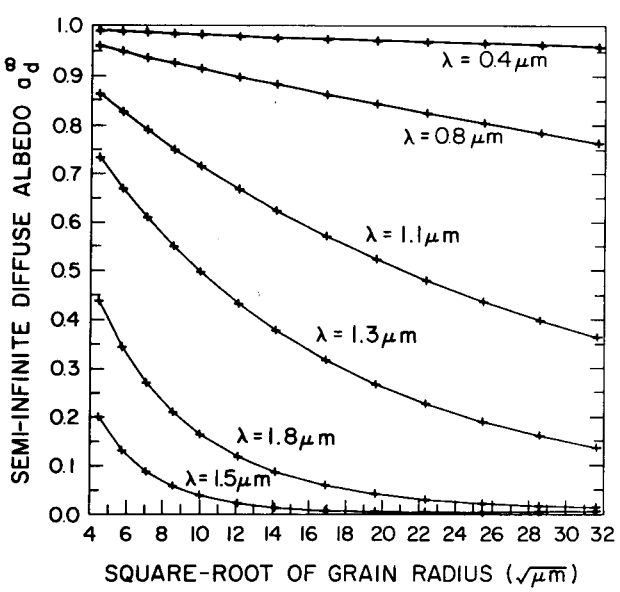

FIG. 9. Diffuse albedo a_d versus square root of grain radius for seven discrete wavelengths.

b. *Effect of liquid water content*

Field experience indicates that snow albedo decreases as the liquid water content increases (e.g., Grenfell and Maykut, 1977). We can speculate about the reason for this. Liquid water replaces air between ice grains (Colbeck, 1975; 1979). The spectral refractive index of liquid water is very close to that of ice for $\lambda < 5\ \mu$m (Irvine and Pollack, 1968, Figs. 1, 2). The replacement of air by liquid water between ice grains can thus increase the effective grain size. (This argument does not apply to the microwave part of the electromagnetic spectrum. There m_{ice} and m_{water} differ considerably, leading to dramatic differences in microwave emissivity between wet and dry snow.)

There is some observational evidence for this view that the liquid water reduces snow albedo only by increasing the effective grain size. We reproduce here (Fig. 10) a figure from O'Brien and Munis (1975, their Fig. 9).[4] They observed the spectral albedo of a snow sample to be lower after warm air

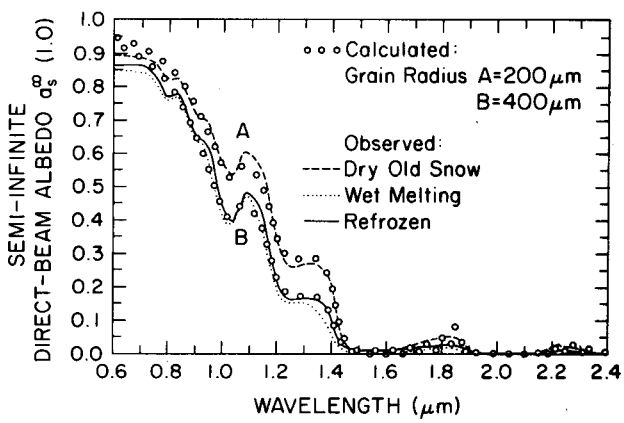

FIG. 10. Comparison of calculated spectral albedo with laboratory measurement of snow reflectance; effect of liquid water content. Observations are taken from O'Brien and Munis (1975)[4] but corrected by us for the reflectance of the $BaSO_4$ standard they used.

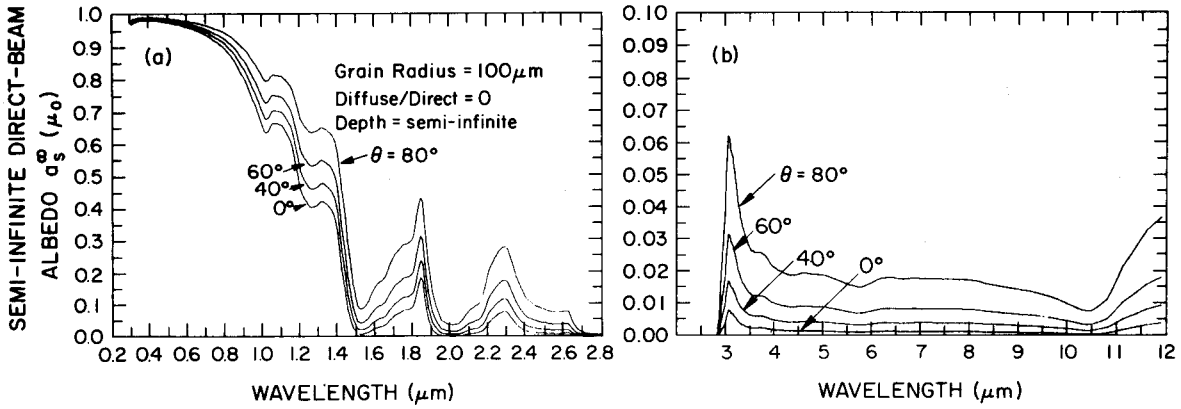

FIG. 11. Semi-infinite direct-beam albedo $a_s^\infty(\mu_0)$ versus wavelength for several values of direct-beam zenith angle $\theta = \cos^{-1}\mu_0$.

had been blown over it so that the surface was wet. But there was no further change in albedo when the sample was refrozen. There was then no liquid water present, but the water bridges between grains had presumably frozen, with no change in the effective grain size.

In addition to changing the effective grain size by its mere presence, liquid water also speeds up the *rate* of grain growth. This explains why only a short exposure to melting conditions can reduce the albedo considerably.

c. *Dependence on solar zenith angle*

In Section 4c we plotted a number of observations of the sun-angle dependence of snow albedo and saw that they were not inconsistent with our model predictions. But those predictions were not spectrally-integrated whereas some of the observations were. Also, many instruments do not exhibit a proper "cosine-law" response at large zenith angles (Dirmhirn and Eaton, 1975), which leads them to consistently overestimate the albedo at such zenith angles. Another cause of increase in albedo with zenith angle which we have not considered in our model is specular reflection at glancing incidence from a thin ice layer ("firnspiegel") which is sometimes present. Middleton and Mungall's (1952) measurements indicate a definite specular reflection developing near grazing incidence for glazed crust. This may account for observations (e.g., Hubley, 1955) showing that, in early morning when an ice crust is sometimes present due to nighttime refreezing of meltwater, the albedo is higher than at the *same* solar zenith angle in late afternoon. Thus, while we consider that our model furnishes useful predictions of the sun-angle dependence, we realize that neither they nor the measurements are definitive.

Fig. 11 shows our calculated spectral albedo $a_s^\infty(\mu_0)$ for direct solar radiation at zenith angles from 0 to 80°. The albedo increases at all wavelengths as the zenith angle increases. Relative to direct overhead sun, the albedo increases only a few percent in the visible but by as much as 0.2 in the near-IR. It is clear that albedo changes most rapidly with θ_0 at large values of θ_0. This is because θ_0 enters our equations only as $\mu_0 = \cos\theta_0$, which changes slowly for small θ_0. This explains Petzold's (1977) empirical rule-of-thumb that snow albedo is virtually independent of θ_0 for $\theta_0 < 50°$.

Our calculations are for a flat snow surface. Because of suncups on temperate glaciers (e.g., Post and LaChapelle, 1971, Figs. 85–88), sastrugi on polar glaciers, and other surface features, the effective zenith angle probably rarely reaches 80°. The nonplanarity of the snow surface will play a much greater role at grazing incidence. Surface elements with a larger μ_0 than the planar value will tend to contribute more to the average or effective value of μ_0 than those with μ_0 less than the planar value, because the latter will more often be in shadow and so contribute nothing. Hence the average μ_0 will be smaller than the planar value. [In the South Polar region, fields of oriented sastrugi ridges can cause a local diurnal cycle of albedo of ~3% even though the solar zenith angle is constant throughout the day (M. Kuhn, personal communication).] Furthermore, as the sun goes to very high zenith angles, the incident radiation becomes dominated by sky radiation rather than direct radiation, so the effective zenith angle becomes less than the solar zenith angle. This should lead to a peak in the albedo as a function of θ_0 rather than a simple monotonic increase all the way to $\theta_0 = 90°$.

In Fig. 11b we have continued the albedo calculation out to $\lambda = 12$ μm, to show the albedo peak at 3.1 μm discussed earlier and also the behavior of directional snow emissivity $\epsilon_s(\mu)$ [Eq. (9)]. In the atmospheric window region ($8 \leq \lambda \leq 12$ μm), we see that a decrease of emissivity toward grazing

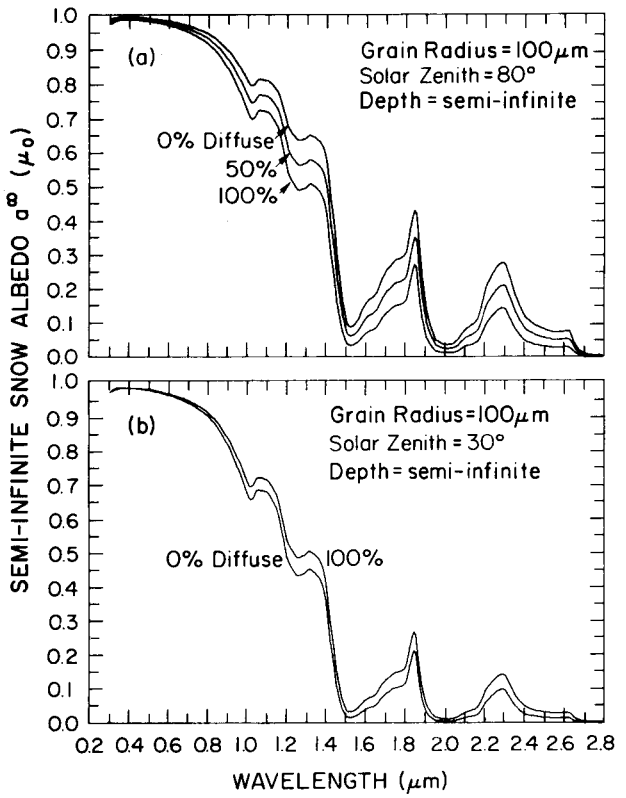

FIG. 12. Semi-infinite net albedo a^{∞}_{net} versus wavelength for various ratios of diffuse to direct radiation.

angles is predicted. For example, at $\lambda = 12$ μm, $\epsilon_s = 0.963$ for $\theta_0 = 80°$ increasing to 0.996 for $\theta_0 = 0°$. Also, the emissivity decreases steeply between 10.5 and 12 μm. Remote sensing over snow in the infrared window region may have to account for such nonunit emissivities and their spectral and angular variation.

d. *Effects of cloud cover*

Cloud cover influences snow *spectral* albedo by converting direct radiation into diffuse radiation and thus changing the effective zenith angle. Eq. (8) allows the calculation of albedo for any given ratio of diffuse to direct incidence. Fig. 12 shows some results from this equation. In Fig. 12a we see that when $\theta_0 = 80°$, the albedo is *reduced* when the diffuse fraction is increased. This is because the purely diffuse radiation has an effective zenith angle near 50°; thus, converting direct into diffuse radiation reduces the effective zenith angle, thereby reducing the albedo.

When the sun is high the effect of cloud cover is just the opposite. Fig. 12b shows that for $\theta_0 = 30°$ conversion of direct into diffuse radiation slightly increases the albedo. Near $\theta_0 = 50°$ the formation of cloud cover would leave spectral show albedo virtually unaltered.

For the *spectrally integrated* albedo, one must also consider that clouds change the spectral composition of the radiation incident on the snow. They cause the radiation field to become relatively richer in visible wavelengths. This tends to increase the snow albedo, which acts counter to the zenith angle effect for $\theta_0 > 50°$ (typical of snow-covered regions). That the visible-enrichment effect almost always wins out is indicated by numerous observations (e.g., Liljequist, 1956). But that the zenith-angle effect is operative is indicated in Rusin's (1961, Table 173) Antarctic measurements; he found the spectrally-integrated albedo to increase only from 0.83 (clear) to 0.90 (overcast) at $\theta_0 = 80°$, while it increased all the way from 0.74 to 0.93 when $\theta_0 = 45°$.

e. *Dependence on snowpack thickness*

The albedo of a thin snowpack obviously depends upon the albedo of the underlying surface; only when the snowpack becomes thick enough are the effects of the underlying surface obliterated. Here we shall examine just how thick a snowpack must be before it can be regarded as "effectively semi-infinite."

Eq. (1) indicates that, because of the inverse dependence of optical depth on grain radius r, radiation will penetrate deeper into a pack of larger particles if the density ρ is kept fixed. This can be seen immediately in Fig. 13, which shows calculated spectral albedo for various snowpack thicknesses (given in liquid water equivalent) with a black underlying surface. Beyond $\lambda = 2.8$ μm less than 1 mm is required to make the pack optically semi-infinite, and indeed beyond about $\lambda = 1$ μm it seems unlikely that the effect of finite thickness will ever be seen. The thin-snowpack albedos differ substantially from the semi-infinite case only in the visible region where the radiation penetrates to much greater depths than in the near infrared.

The liquid-equivalent depth for which the snowpack becomes effectively semi-infinite (i.e., albedo at all wavelengths within 1% of that for an infinitely-thick snowpack) is 2 cm for grain radius $r = 50$ μm (e.g., 20 cm of fluffy new snow, $\rho = 0.1$ g cm^{-3}), about 8 cm for $r = 200$ μm (e.g., 20 cm of fine-grained old snow, $\rho = 0.4$) and 20 cm for $r = 1000$ μm (e.g., 50 cm of old melting snow of $\rho = 0.4$). This means that as a snowpack of less than 20 cm liquid equivalent ages and the grain size increases, so that the pack's optical thickness decreases, one may eventually "see" the ground through it even in the absence of melting and runoff. Thus, two snowpacks, one of which becomes optically finite as grain size increases while the other does not, will show differing albedo time series even if their grain size time series are identical.

Our results as to what constitutes semi-infinite snow are in general agreement with some other investigators. Schlatter (1972), based on an examination of Antarctic snow measurements, indicates at least $d = 50$ cm is necessary. Bergen (1975) indicates a figure of $d = 30$ cm, while Grenfell (1979) indicates $d = 10$–20 cm. These investigators were considering snows which differed greatly in density and grain size, and an examination of Fig. 13 shows how they could come up with differing numbers.

However, our calculations fail to explain the dependence of albedo on depth found by Giddings and LaChapelle (1961, Fig. 2). For $\lambda = 0.59$ μm and $r = 250$ μm, their measured albedo rose rapidly as thickness increased to 2 cm. At 2 cm the albedo was within 3% of the asymptotic limit. In Fig. 13b our calculations are for grains near this size ($r = 200$ μm) and at $\lambda = 0.59$ μm we appear to need 3 cm of liquid-equivalent depth to obtain an albedo within 3% of the asymptotic limit. For a density we guess to be 0.4, this is a geometric depth of 7.5 cm, i.e., 4 times as deep as the experiment showed. This discrepancy is addressed in Part II (Warren and Wiscombe, 1980).

An interesting effect of finite depth is that it considerably flattens the spectral albedo curves between $\lambda = 0.3$ μm and $\lambda = 0.8$–0.9 μm. This may explain several observations (see Mellor, 1977) showing very flat spectral snow albedos.

f. Effect of snow density on albedo

Some investigators find snow albedo to be a function of snow density (e.g., Arai, 1966; Bergen, 1975). O'Brien and Munis (1975)[4] also noticed that an increase in density correlated with a decrease of albedo, but they cautioned that density was often correlated with other symptoms of aging, such as grain size, and were skeptical as to whether density per se influenced albedo.

Our calculated albedo does not depend upon density. One would expect this to be true as long as curves like those of Mellor (1977) for flux extinction coefficient are about linear in density, which is true up to densities of ~0.4 g cm^{-3}. Beyond that density, shadowing of grains and other near-field phenomena could introduce a dependence of albedo on density. This matter is discussed further in Section 7.

Bohren and Barkstrom's (1974) formula for snow albedo also does not involve the density, and Bohren and Beschta (1979) have done a relevant experiment. They measured spectrally integrated albedo (0.35–2.8 μm) of a snowpack immediately before and after running a snowmobile over it. The compaction by the snowmobile increased the density, from 0.05 to 0.20 g cm^{-3} or from 0.30 to 0.45 g cm^{-3}, but there was insufficient time between measurements for the grain size to change, and the change in albedo was insignificant.

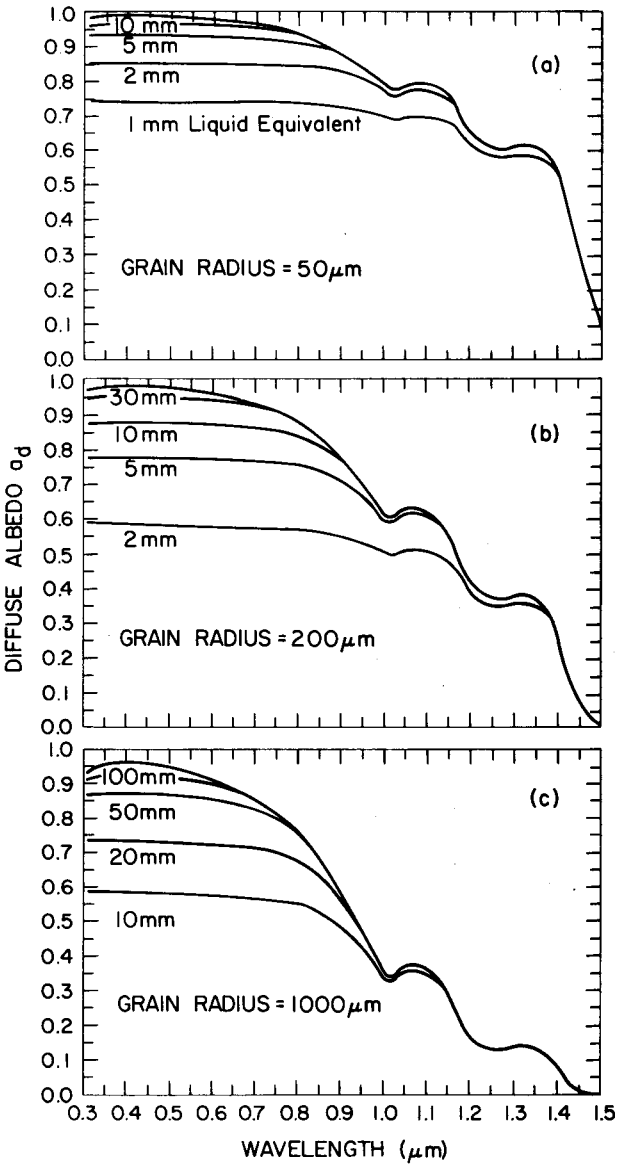

FIG. 13. Direct beam albedo $a_s^*(\mu_0)$ versus wavelength for various grain radii; and, for each grain radius, for a variety of snow depths expressed in liquid equivalent. The top curve in each case is for semi-infinite depth.

g. Sensitivity of albedo calculation to error in absorption coefficient

We pointed out in Section 4a that in some spectral regions different values of ice imaginary refractive index m_{im} have been obtained by different investigators. Fig. 14 shows the spectral albedo calculated for our standard snowpack, with m_{im} everywhere multiplied by 0.5, 1, 2, 5 or 10 for all $\lambda \leq 2.0$ μm. (For $\lambda > 2.0$ μm we think there is little uncertainty.)

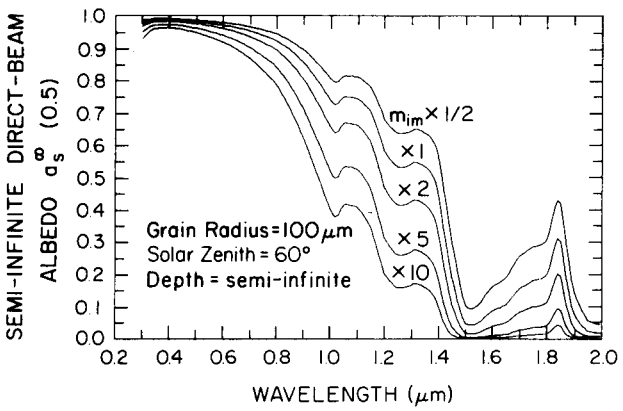

FIG. 14. Sensitivity of spectral albedo calculation to error in absorption coefficient of ice.

For $0.33 \leq \lambda \leq 0.45$ μm, Kalitin's (1936) values for m_{im} are about 10 times as large as Sauberer's (1950), which we used. This difference is seen to reduce the albedo by only 2–3%. For longer wavelengths the sensitivity of albedo to error in m_{im} becomes more pronounced, but the uncertainty in m_{im} is less beyond about $\lambda = 1$ μm (typically no more that a factor of 2). It can be seen that the strange "finger" in the albedo curve near $\lambda = 1.85$ μm, which as we discussed earlier is not observed, would be eliminated if m_{im} would be multiplied by factors ranging from 1 to 2 in the region $1.80 \leq \lambda \leq 1.86$ μm.

6. Comparison of calculations with observations of snow reflectance

a. Near-infrared

O'Brien and Munis (1975)[4] made laboratory measurements of the bidirectional spectral reflectance of natural snow. Their measurements were relative to a $BaSO_4$ standard, so we took their raw values and corrected them for the diffuse reflectance of $BaSO_4$ (Grum and Luckey, 1968). Their snow thicknesses were always in the range 10–20 cm, which is sufficiently thick that the albedo is within 1% of that of a semi-infinite snowpack, as we showed in Section 5e, except possibly for old melting snow. Figs. 10 and 15 are typical of their results, which were for a source zenith angle of 0° and detector zenith angle of 30°.

Curve A of Fig. 15 was from a sample of fresh snow, and Curve B from a sample of the same snowfall after two days of natural aging at temperatures hovering above and below freezing. We are able to fit these curves with our albedo function $a_s(1)$ (dashed lines) for $r = 50$ μm and $r = 200$ μm although there are significant disagreements. The calculated albedo falls below the reflectance measurements for $\lambda < 1.2$ μm. The calculated peak at 1.1 μm is not sharp enough. The peak at $\lambda = 2.3$ μm is shifted to higher wavelength relative to the observation. And at $\lambda = 1.85$ μm there is a spike in the calculated albedo which does not appear in the measurements, although we have given what we think is the correct explanation of this problem in Section 5g.

At the other wavelengths, there are several factors which may be contributing to the disagreements we see:

1) Our calculated albedo a_s^∞ ($\mu_0 = 1$) corresponds to the *integral* of O'Brien and Munis's bidirectional reflectance over all detector angles (weighted by cosine of detector angle). They tried different source and detector angles, although only out to 30° at most; the variability they found with detector angle is large enough and in the right direction to explain most of the disagreements, especially for $\lambda < 1.2$ μm. We might note that spectrally detailed near-infrared reflectance measurements over snow are rare indeed; thus, while it is less than desirable to compare directional albedo with bidirectional reflectance, the comparison at least validates the performance of the model in a broad sense.

2) Experimental error is estimated to be ~5% by O'Brien and Munis, but it grows worse as one approaches the visible, as indicated by the unrealistic erratic oscillations in their curves starting at $\lambda = 0.75$ μm.

3) Values of ice absorption are still uncertain by up to 20–50% at some near-IR wavelengths. However, as can be seen in Fig. 14, it would take a factor of 2 decrease in ice imaginary index at $0.6 \leq \lambda \leq 1.2$ μm to bring calculation into agreement with observation, and this seems unrealistic.

4) The factor for conversion from reflectance relative to $BaSO_4$ powder to true reflectance is still not entirely agreed upon for $0.3 \leq \lambda \leq 0.7$ μm (Patterson *et al.*, 1977). But the disagreement is at

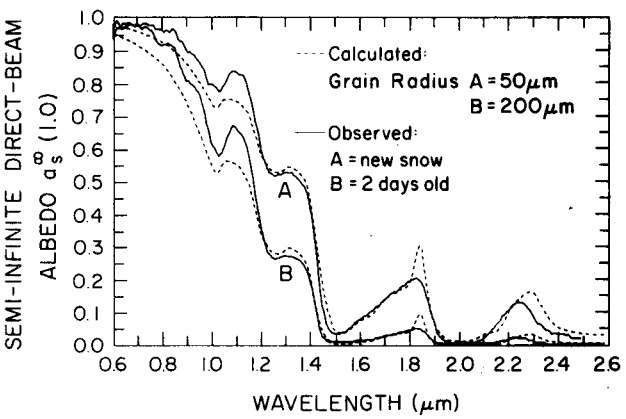

FIG. 15. Comparison of calculated spectral albedo with O'Brien and Munis laboratory observations of snow reflectance.

the 3% level. The reflectance of O'Brien and Munis's $BaSO_4$ standard would have to differ by up to 10% from accepted values to explain completely the discrepancies in Fig. 15.

However, the size (and even the sign) of the discrepancy between our calculation and O'Brien and Munis's observation is different for different snow samples. Fig. 10 shows results for a snow sample that was taken through a melting and refreezing cycle compared to our calculated $a_s^\infty(1)$ for $r = 200$ and 400 μm, which gives the best fit for $\lambda \geq 1.2$ μm. Here our calculation *overestimates* the measurements for $\lambda \leq 0.85$ μm by up to 0.05. This suggests that reasons (1) and (2) above are the major contributors to the discrepancies. However, in both Figs. 10 and 15 our calculation is seen to underestimate the peak at $\lambda = 1.1$ μm. This is possibly due to an error in the measured m_{im} of ice. m_{im} for liquid water is about a factor of 2 lower at its local minimum here. Fig. 14 shows that a factor of 2 error would be the right size to explain this discrepancy.

Overall, it may be said that our model furnishes a respectable simulation of near-infrared spectral snow albedo. It is capable of matching a large number of data points by adjusting but a single parameter—the effective grain size. Furthermore, the values of grain size selected are entirely in concord with the known range of grain sizes for fresh, middle-aged and old snow (see Section 3b).

b. Visible

Fig. 16, which we have reproduced from Mellor's (1977) review article, summarizes some field measurements of spectral snow albedo in the visible. They obviously agree neither in magnitude nor trend. The measurements of Thomas, which increase monotonically, particularly lack credibility. Those of Krinov were made in the 1930's in Russia with instruments of uncertain accuracy. Rarely was grain size, or even the age or state of the snow surface, specified very well if at all. This goes also for many measurements not shown in Fig. 16.

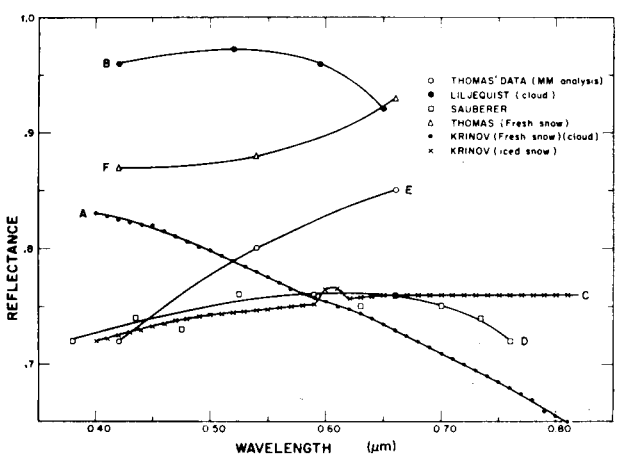

FIG. 16. Reflectance of snow as a function of wavelength in the visible, according to various investigators. From Mellor (1977).

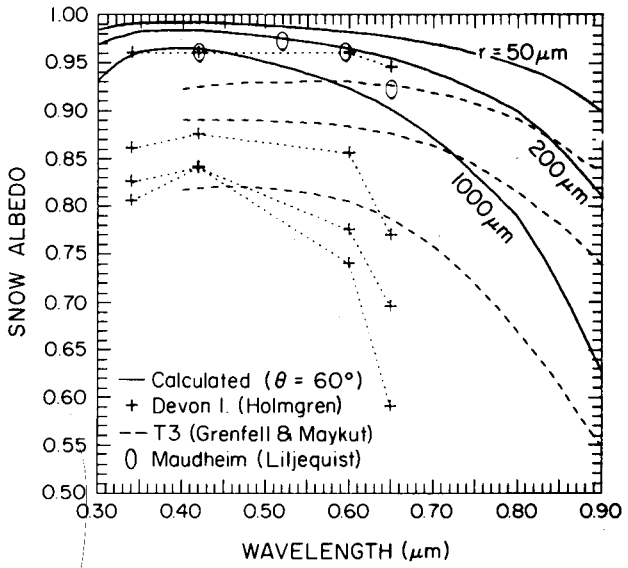

FIG. 17. Spectral albedo of snow in the visible, comparisons of calculation with observations.

For comparison with our calculations, we have selected some observations made with good instruments under well-defined conditions, which are plotted in Fig. 17. Liljequist (1956) measured snow albedos at four visible wavelengths at Maudheim, on a small ice shelf at the coast of Antarctica, during the period 1949–52. He made his observations under overcast conditions so that errors could not be introduced by possible lack of a cosine-law response in his instrument. The albedos for this dry fine-grained snow were among the higher ever obtained, dropping from 97% at $\lambda = 0.52$ μm to 92% at $\lambda = 0.65$ μm. These reported values are averages of measurements made on five different days for different snow conditions. (The range between high and low values at each wavelength was 0.6–2.3%.) Holmgren (1971) measured albedos at four visible wavelengths at Devon Island in the Canadian Archipelago (75°N) in summer 1962. In order of decreasing albedo, the four curves are (a) new loose snow on top of hard wind-packed snow, (b) frozen snow over wet melting snow, (c) melting well-drained snow and (d) melting soaked snow. Grenfell and Maykut's (1977) observations are for snow at Ice-island T3 in the Arctic Ocean. In order of decreasing albedo, they are dry cold snow, wet new snow and melting old snow. They used the portable spectrophotometer designed by Roulet *et al.* (1974). Its spectral resolution was good, being at worst ~0.2 μm (at $\lambda = 0.9$ μm).

The calculated albedos (solid lines) are for $r = 50$, 200 and 1000 μm, respectively. They are taken from Fig. 8. The calculation was for direct incidence at $\theta = 60°$, but the curves would be insignificantly different for diffuse incidence. The calculated albedos for new snow ($r = 50$ μm) exceed those measured by Holmgren and Liljequist by 2–6%. They disagree even more with the top curve of Grenfell and Maykut, but these measurements were for "wind-packed" snow, not necessarily new, of undetermined grain size. While the discrepancy between observation and calculation for *new* snow might possibly be explained by observational error, this cannot be said for old and melting snow. The model is clearly calculating unreasonably high albedo values for old and melting snow. This failure of the model in the visible region is in clear contrast to its success in the near-IR, where the decrease in albedo with aging was seen to be adequately described by the increase in grain size in the model. The value of m_{im} is so small in the visible that an increase in grain radius to 1 mm fails to reduce the albedo (at $\lambda = 0.4$ μm) below 96%. Snow grains are rarely larger than $r = 1$ mm, but even the use of an unreasonably large grain size ($r = 4$ mm) fails to reduce the calculated albedo (at $\lambda = 0.4$ μm) below 92%.

There are several possible explanations for the discrepancies:

1) The effects of nonsphericity and/or close packing of snow crystals can be ignored in the near-infrared where m_{im} is large but become important when m_{im} is small. This possibility is discussed in Section 7.

2) Our values of m_{im} in the visible may be too small. But they would have to be 3–40 times larger (40 at $\lambda = 0.4$ μm, smaller factors for larger λ) to mimic the observations. Kalitin (1936) indeed reported values of m_{im} 6–10 times larger than ours (Sauberer, 1950) in the spectral range $0.33 \leq \lambda \leq 0.45$ μm, but all in all we think Sauberer's values are more reliable. If anything, Sauberer's values should be too *large*, because he used lake ice rather than pure ice. Furthermore, the m_{im} of *liquid* water, which is more easily measured than that of ice, also reaches such low values as 7×10^{-10} (Patel and Tam, 1979; Tam and Patel, 1979). This is a factor of 2 *smaller* than our minimum m_{im} for ice. Since at longer wavelengths the m_{im} of ice and water do not differ by more than a factor of 6, and this only because of shifts in band positions (Irvine and Pollack, 1968), it seems unlikely that they could differ by a factor of 40 at $\lambda \approx 0.4$ μm. Still, we would suggest a careful remeasurement of m_{im} in the visible as a high-priority task.

3) We also considered whether the snow used for the measurements in Fig. 17 was effectively semi-infinite. Finite depth would provide just the effect we see: a reduced albedo in the visible but no change in the near-IR (Fig. 13). But it turns out that for only one of the curves in Fig. 17 can the low albedo be partly due to insufficient depth. This is the middle curve of Grenfell and Maykut (1977) which was for ~2 cm (liquid equivalent) of snow on top of white ice; we examine this situation in detail in Part II. Their other two samples were thick snowpacks, and the samples of Liljequist (1956) and Holmgren (1971) were certainly semi-infinite, being an ice shelf and a glacier, respectively.

4) The remaining possibility is that the small amounts of absorptive impurities present in natural snow can effectively reduce the visible albedo. [Dunkle and Bevans (1956) and Giddings and LaChapelle (1961) both mention this effect as a possibility but they present no estimates or calculations of it, and in fact Giddings and LaChapelle dismiss it as unimportant.] The effect of impurities is examined in Part II (Warren and Wiscombe, 1980).

7. Effects of close packing and nonsphericity

a. Close packing

The Mie scattering calculations are for a plane electromagnetic wave incident on a single isolated sphere of ice. Spheres in an assemblage will retain the single-scattering properties ($\tilde{\omega}, g, Q_{\text{ext}}$) that they would have in isolation, provided that they are not in a regular array, and that they are not in each other's "near field." They must be sufficiently far apart that 1) interparticle interference effects are negligible; 2) each grain is exposed to an incident plane wave; and 3) grains do not shadow one another. Cloud droplets, for example, would be sufficiently far apart that near-field effects would not appear. In a snowpack the individual grains are not in a regular array, but they are close together, so we must fact the possibility that our Mie calculations do not correctly give the single-scattering properties. Specifically, we want to know whether our model's failure to match observations of visible snow albedo is due to its neglect of near-field effects.

It should be noted that the far-field assumption is made only in that part of our model using Mie theory. The δ-Eddington approximation for multiple scattering (as well as other radiative transfer methods, such as the diffusion approximation used by Giddings and LaChapelle, 1961) should be applicable to radiative transfer in a close-packed medium, as long as it is provided with appropriate single-scattering quantities.

1) Interparticle interference

The breakdown of the far-field approximation as the density increases has been documented experi-

mentally for closely packed particles with size parameter $x \approx \lambda$. Blevin and Brown (1961) studied suspensions of submicron-diameter pigment particles in water or air. The reflectance at visible wavelengths ($0.4 \leq \lambda \leq 0.7$ μm) for an optically semi-infinite suspension of $MgCO_3$ particles in air was found to be independent of density up to a volume concentration of 30%, but to decrease with further increase in volume concentration. This is what one might expect for these small particles: as the density increases, the interparticle separation is reduced to the order of a wavelength, so adjacent particles scatter more and more coherently. The scattering behavior of two adjacent particles may approach that of a single larger particle (Vedernikova and Kabanov, 1974), reducing $\tilde{\omega}$ and/or increasing g, both of which would reduce the albedo.

A simple device (Heller, 1945; Hiltner and Krieger, 1969) which has been used to correct Mie calculations for this near-field effect is to replace the refractive index of the surrounding medium by a volume-weighted average of the refractive indices of the medium and the suspended particles. Gate (1973) measured the volume scattering coefficient of dense suspensions of polystyrene spheres in water as a function of volume concentration, wavelength (visible), and particle size. He obtained good agreement with almost all of his experimental data by taking the effective refractive index of the surrounding medium not as that of pure water but rather as

$$m_{\mathrm{re}}^{\mathrm{med}} = (1 - v)m_{\mathrm{re}}^{w} + vm_{\mathrm{re}}^{s}, \tag{11}$$

where

v volume-fraction of spheres
m_{re}^{s} real refractive index of spheres
m_{re}^{w} real refractive index of water.

Then for his Mie calculations he used

$$\left.\begin{aligned} m_{\mathrm{re}} &= m_{\mathrm{re}}^{s}/m_{\mathrm{re}}^{\mathrm{med}} \\ x &= 2\pi r m_{\mathrm{re}}/\lambda \end{aligned}\right\}, \tag{12}$$

where λ is the wavelength in vacuum.

The results of employing such an adjusted m_{re} in our model for snow were that Q_{ext} and $\tilde{\omega}$ both decreased insignificantly, but g increased considerably.

The insensitivity of $\tilde{\omega}$ to the presence of nearby spheres seems plausible from a geometrical optics viewpoint. $(1 - \tilde{\omega})$ is the ratio $Q_{\mathrm{abs}}/Q_{\mathrm{ext}}$. Q_{abs} is determined almost entirely by rays passing *through* the sphere (as opposed to edge rays or diffracted rays), and these are not much influenced by nearby spheres, as follows from the very definition of a ray (see Born and Wolf, 1965, Chap. III). Q_{ext}, which is near 2 for large ice grains in the far-field, might be reduced if close-packing caused diffraction to be reduced, as suggested by Sarofim *et al.* (1968).

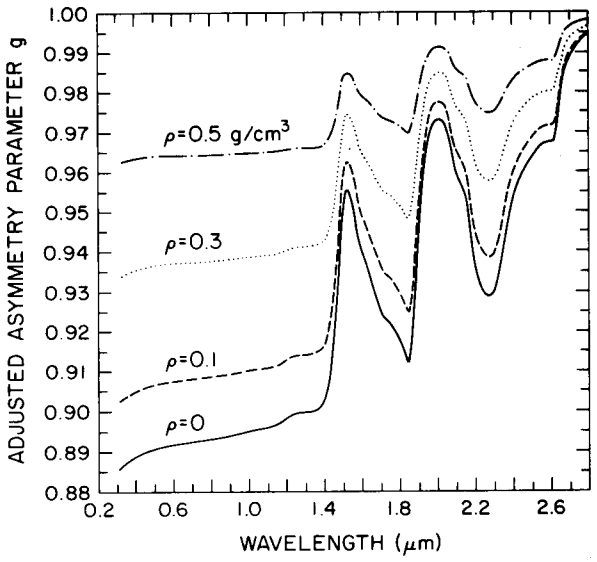

FIG. 18. Near-field test; effect on asymmetry parameter of adjusting the refractive index of the surrounding medium (air) using Eq. (11).

But even if diffraction were to disappear completely, Q_{ext} would approach 1 and thus $(1 - \tilde{\omega})$ would be increased only by a factor of 2, not the factor of 50–100 which we would need to reduce calculated visible albedo to observed values. (From Figs. 3 and 8 it can be seen that at $\lambda = 0.4$ μm, an increase in $(1 - \tilde{\omega})$ by a factor of 20 reduces the albedo by only 3%.) This relative insensitivity of $\tilde{\omega}$ to m_{re} is also in concert with an approximation of Sagan and Pollack (1967), which comes from the lowest order truncation of the geometrical optics formula, showing that $\tilde{\omega}$ is a function only of m_{im}.

For the asymmetry factor g, Fig. 18 shows the results of Mie calculations using the adjusted m_{re} of (11) and (12), for snow ($r = 200$ μm) of density $0 \leq \rho \leq 0.5$ g cm^{-3}. For all wavelengths the scattering becomes more forward-directed. In the visible, g increases from 0.89 in the far-field limit to 0.96 for $\rho = 0.5$ (near the upper limit for the density of a surface snow layer).

Since the major effect of this adjustment in $m_{\mathrm{re}}^{\mathrm{med}}$ was to increase g, we calculated snow albedo for $r = 200$ μm (Fig. 19) using specified values of g higher than that calculated for the far-field limit. Raising g to a uniform value of 0.96 for $0.3 \leq \lambda \leq 1.5$ μm decreases the albedo considerably in the near-IR but only by 1–2% at $\lambda = 0.4$ μm. Even when we use a ridiculously large asymmetry parameter ($g = 0.99$) the reduction in albedo at $\lambda = 0.4$ μm is only 4%.

This possible near-field effect, therefore, is dramatically inadequate to explain our discrepancy with observations of visible albedo. Furthermore, to agree with observations, we require our calculated

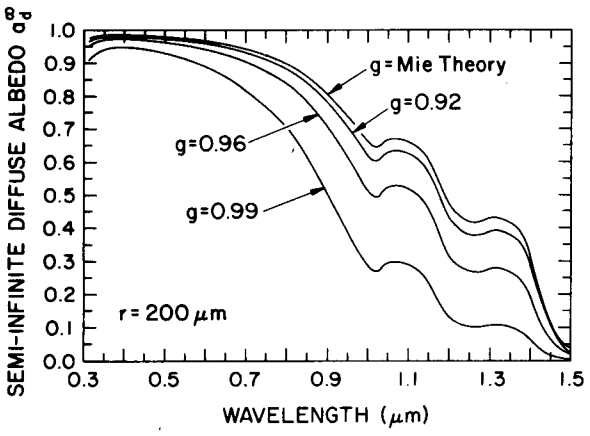

FIG. 19. Effect on snow albedo of artificially raising asymmetry parameter g.

albedo to be reduced only in the visible, not in the near-IR. This form of a near-field correction does just the opposite and, in fact, up to $\rho = 0.5$ has an effect similar to that of increasing the grain size in our model (Fig. 8), so if this near-field effect is operative in snow we could probably mimic observations simply by increasing the grain size. This could account for the fact that in Fig. 7 of Part II we require a grain size $r = 1300\ \mu$m to match Grenfell and Maykut's (1977) albedo measurement at $\lambda = 0.9\ \mu$m for old melting snow, whereas they measured the grain size to be smaller, $r = 500\ \mu$m.

However, there is reason to think that interparticle interference is insignificant for shortwave radiation in a snowpack. The experiments of Blevin and Brown (1961) and Gate (1973), as well as other experiments on pigments, paints and polystyrene spheres which showed a dependence of albedo on density (e.g., Harding *et al.*, 1960; Hottel *et al.*, 1971) all involved particles of size r close to the wavelength λ. At high density the interparticle separation δ is also close to the wavelength ($r \approx \delta \approx \lambda$). The interparticle separation between grains in a snowpack, although small relative to the radius r, would still be large relative to the wavelength ($r \approx \delta \gg \lambda$), so they would not be likely to scatter coherently.

2) NONPLANE WAVE

A particle in the near field of another particle is not irradiated by a plane electromagnetic wave. The path lengths and directions of photons passing through a particle in the near field of another will be different than in the far-field case. This will alter g and $\tilde{\omega}$, but not by nearly enough to resolve our visible albedo problem. We saw above (Fig. 19) that even an unreasonably large g had little effect on the visible albedo. $(1 - \tilde{\omega})$ would be increased in the same proportion that the average photon path length through the particle was increased. (The absorption coefficient in the visible is so small that absorption is nearly linear in path length.) It is difficult to imagine that the difference in average photon path length due to an impinging non-plane wave could be as much as a factor of 2, but we would need even a much greater factor (50–100) to bring the calculated albedo down to the values observed. This appears impossible.

In addition to these arguments, there is an experimental reason for considering near-field effects (i) and (ii) to be relatively small in snow. The experiments of Bohren and Beschta (1979), described in Section 5f, show that the albedo of snow, unlike that of the pigments studied by Blevin and Brown (1961), did not decrease significantly with increasing density (and fixed grain size) up to $\rho = 0.45$ g cm^{-3}.

3) SHADOWING

Shadowing of snow grains by one another reduces the optical depth τ as calculated from (1), since all N grains will not contribute their full cross-section σ_{ext}. Thus light may penetrate to greater liquid-equivalent depths as snow densifies. On the assumption (which is of course only a crude approximation) that a grain is either completely shadowed or completely unshadowed, neither $\tilde{\omega}$ nor g would be affected by shadowing. In this case, shadowing would reduce the albedo of a *thin* snowpack only, so it could not account for the discrepancy between theory and observation for semi-infinite snow.

We think it is quite possible that shadowing does reduce the albedo of a thin snowpack. Brillouin [1949, Eq. (5) and Fig. 2], using very crude physical optics considerations, derived that the region of complete shadow (umbra) should extend a distance $R \sim r^2/2\lambda$ when $\lambda \ll r$. According to this criterion, shadowing occurs at all solar wavelengths for all grain sizes and densities present in natural snow. The effect of shadowing has been observed for particles in paint by Blevin and Brown (1961), who commented ". . . very high pigment concentration in a paint layer can cause a decrease in its opacity or hiding power." Shadowing cannot be ruled out as a potential explanation for the discrepancy between measurement and observation. But the direction of its effect on the albedo of deep snow, and whether it would affect the visible more than the near-IR albedo, is at present not at all clear.

b. Nonsphericity

Experiments (e.g., Zerull, 1976) have shown that the sphericity assumption is sometimes adequate for describing scattering by ensembles of nonspherical particles. It becomes worse for larger and/or

highly irregular particles. The details of the angular scattering pattern (phase function) are the most sensitive to nonsphericity; generally sidescattering is enhanced while backscattering is depressed relative to spheres. The cross sections for absorption and scattering are likely to be much less sensitive to nonsphericity than is the phase function at specific angles.

Mugnai and Wiscombe (1980) have studied these cross sections theoretically for randomly oriented moderately nonspherical particles and find them to be quite close to those for equal-volume spheres. In the semi-empirical theory of Pollack and Cuzzi (1980), the absorption cross section is unaltered (from its equal-volume sphere value) while the scattering cross section is increased by the ratio

$$r = \frac{\text{total surface area of irregular particles}}{\text{total surface area of equal-volume spheres}}.$$

Since

$$1 - \tilde{\omega} = \sigma_{\text{abs}}/\sigma_{\text{sca}}$$

to an excellent approximation for snow at $\lambda \leq 0.9\ \mu$m, we would have

$$(1 - \tilde{\omega})_{\text{nonspherical}} = \frac{1}{r}(1 - \tilde{\omega})_{\text{spherical}},$$

according to the Pollack/Cuzzi theory. r is not likely to be larger than 3 for typical snow grains, and a factor of 3 reduction in $(1 - \tilde{\omega})$ will have little effect (less than 1%) on our visible albedo calculations. But in any case the reduction in $(1 - \tilde{\omega})$ caused by nonsphericity is exactly opposite in direction to what we need; a 50–100-fold *increase* is required to explain our disagreement with observations.

It might be noted that Hansen and Pollack (1970) assumed ice spheres in modeling the reflectivity of thick ice clouds and found agreement with laboratory measurements even though cloud ice particles are even more irregular than snow grains. Thus the nonsphericity corrections, while certainly real, are probably small.

In a situation similar to ours, near-field and nonsphericity effects were ignored with impunity by Conel (1969). He used the Chandrasekhar two-stream approximation and Mie scattering theory to predict spectral emissivity of mineral dust. He was able successfully to predict many of the IR spectral emissivity features of nonspherical close-packed quartz powders in various states of granulation.

Independent of the above arguments, there is a reason sufficient in itself to show that neither close-packing nor nonsphericity significantly reduces visible snow albedo (except for shadowing in thin snowpacks). Very high values of visible albedo, such as our model predicts, are indeed sometimes observed in dry compact snow. These are the measurements of Liljequist (1956), $a_d = 97\%$ at $\lambda = 0.52\ \mu$m in Antarctica; and of Bryazgin and Koptev (1969), 93% for 0.4–1.0 μm in the Arctic Ocean. The fact that *some* measurements of snow albedo approach the theoretical values would cast suspicion on a nonsphericity and/or near-field explanation, since if such mechanisms are operative one cannot expect them to be just intermittently operative.

8. Summary and conclusions

Use of Mie theory for single-scattering and the δ-Eddington approximation for multiple scattering of solar radiation in a snowpack allows the snow albedo to be calculated over the entire solar spectrum ($0.3 \leq \lambda \leq 5.0\ \mu$m) for diffusely or directly incident radiation at any zenith angle.

The peaks and valleys of the measured spectral albedo of snow coincide with the minima and maxima, respectively, of the measured spectral absorption coefficient. The absorption coefficient of ice is thus a primary determinant of the spectral albedo of snow, and model calculations of spectral albedo can be no better than the measured absorption coefficients used in the model.

Ice is very weakly absorptive in the visible spectrum but has strong absorption bands in the near-infrared so snow albedo is much lower there. The near-IR solar irradiance thus plays an important role in snowmelt and in the energy balance at a snow surface. Furthermore, while the visible albedo (for *pure* snow) is rather insensitive to variations in model parameters, the near-IR albedo is very sensitive to snow grain size and moderately sensitive to solar zenith angle.

The albedo of a thin snowpack is affected by the underlying surface. The depth necessary for the snow to be "effectively semi-infinite" increases with the grain size; for old melting snow it may be ~20 cm liquid equivalent (50 cm snow). Thus, it is important to record the snow depth and density as well as grain size for albedo measurements on snow less than 1 m thick. Snow cover over Arctic sea ice is often thin enough that its albedo may be reduced by the darker underlying ice.

The model calculations agree well with observations in the near-IR. The decrease in albedo due to snow aging can be mimicked by reasonable increases in grain size. In the visible and near-UV, however, the calculated values exceed almost all observed albedos for deep snow. The discrepancy is worst for old melting snow.

Errors due to approximations made by the model cannot explain the discrepancy. The possible adjustments for near-field effects and nonsphericity of snow grains are judged to be an order of magnitude too small to reduce the calculated visible albedo sufficiently. Furthermore, they affect all

wavelengths so that matching of observed visible albedo for a particular grain size would destroy the model's good agreement in the near-IR.

The measured absorption coefficient of ice is unlikely to be in error by more than a factor of 2, whereas a factor of 50 would be needed to bring our high visible albedo calculations down to observed values. (Nevertheless, we would suggest high priority for a remeasurement of the absorption coefficient of pure ice for wavelengths 0.3–2.0 μm.)

We conclude that the model does indeed calculate reasonable albedos for *pure* snow. For natural snow, the measured albedo is often lower (in the visible, but not in the near-IR) than that for pure snow. In Part II of this paper (Warren and Wiscombe, 1980), we attribute this to the presence of absorptive impurities. The best candidate for pure snow would be the Antarctic plateau because of its isolation from contaminants.

Note added in proof. Grenfell and Perovich (1981) have now remeasured m_{im}(ice) for $0.4 \leq \lambda \leq 1.4$ μm, using a 2.3 m long block of ice. The new values differ by at most a factor of 2 from Sauberer's (1950) values. These largest differences are at $0.4 \leq \lambda \leq 0.6$ μm; the minimum in m_{im} is now found at 0.47 μm instead of 0.40 μm. These new values are expected to have only minor effects on our calculated albedos (cf. Fig. 14) but will shift the position of maximum albedo to slightly higher wavelength, possibly in better agreement with Liljequist's (1956) observations (cf. Fig. 17).

Acknowledgments. We thank Thomas Grenfell and Gary Maykut (U. Washington), Malcolm Mellor (CRREL) and Charles Knight (NCAR) for helpful discussions, and Harold O'Brien (CRREL) for giving us details of his experimental measurements.

REFERENCES

Abramowitz, M., and I. A. Stegun, 1965: *Handbook of Mathematical Functions*. Dover Publications, 1046 pp.

Arai, T., 1966: On the relationship between albedo and the properties of snow. *Japanese Progress in Climatology*, Tokyo University of Education, 88–95.

Barkstrom, B. R., 1972: Some effects of multiple scattering on the distribution of solar radiation in snow and ice. *J. Glaciol.*, **11**, 357–368.

Bergen, J. D., 1971: The relation of snow transparency to density and air permeability in a natural snow cover. *J. Geophys. Res.*, **76**, 7385–7388.

——, 1975: A possible relation of albedo to the density and grain size of natural snow cover. *Water Resour. Res.*, **11**, 745–746.

Blevin, W. R., and W. J. Brown, 1961: Effect of particle separation on the reflectance of semi-infinite diffusers. *J. Opt. Soc. Amer.*, **51**, 129–134.

Bode, G., 1909: Das Verhalten des Eises im ultraroten Spektrum. *Ann. Phys.*, **30**, 326–336.

Bohren, C. F., and B. R. Barkstrom, 1974: Theory of the optical properties of snow. *J. Geophys. Res.*, **79**, 4527–4535.

——, and R. L. Beschta, 1979: Snowpack albedo and snow density. *Cold Regions Sci. Tech.*, **1**, 47–50.

Born, M., and E. Wolf, 1965: *Principles of Optics*, 3rd ed. Pergamon Press, 808 pp.

Brillouin, L., 1949: The scattering cross section of spheres for electromagnetic waves. *J. Appl. Phys.*, **20**, 1110–1125.

Bryazgin, N., and A. Koptev, 1969: Spectral albedo of snow-ice cover. *Prob. Arctic Antarc.*, **29–32**, 355–360.

Choudhury, B. J., and A. T. C. Chang, 1979: The solar reflectance of a snow field. *Cold Regions Sci. Tech.*, **1**, 121–128.

Colbeck, S. C., 1975: Grain and bond growth in wet snow. *Snow Mechanics Symposium*, IAHS-AISH Publ. No. 114, 51–61.

——, 1979: Grain clusters in wet snow. *J. Colloid Interface Sci.*, **72**, 371–384.

Conel, J. E., 1969: Infrared emissivities of silicates: Experimental results and a cloudy atmosphere model of spectral emission from condensed particulate mediums. *J. Geophys. Res.*, **74**, 1614–1634.

Dirmhirn, I., and F. D. Eaton, 1975: Some characteristics of the albedo of snow. *J. Appl. Meteor.*, **14**, 375–379.

Dunkle, R. V., and J. T. Bevans, 1956: An approximate analysis of the solar reflectance and transmittance of a snow cover. *J. Meteor.*, **13**, 212–216.

Gate, L. F., 1973: Light-scattering cross sections in dense colloidal suspension of spherical particles. *J. Opt. Soc. Amer.*, **63**, 312–317.

Giddings, J. C., and E. R. LaChapelle, 1961: Diffusion theory applied to radiant energy distribution and albedo of snow. *J. Geophys. Res.*, **66**, 181–189.

Gow, A. J., 1969: On the rates of growth of grains and crystals in South Polar firn. *J. Glaciol.*, **8**, 241–252.

Grenfell, T. C., 1979: The effect of ice thickness on the exchange of solar radiation over the polar oceans. *J. Glaciol.*, **22**, 305–320.

—— and G. A. Maykut, 1977: The optical properties of ice and snow in the Arctic basin. *J. Glaciol.*, **18**, 445–463.

——, and D. K. Perovich, 1981: Radiation absorption coefficients of polycrystalline ice from 400 nm to 1400 nm. Submitted to *J. Geophys. Res.*

Griggs, M., 1968: Emissivities of natural surfaces in the 8- to 14-micron spectral region. *J. Geophys. Res.*, **73**, 7545–7551.

Grum, F., and G. W. Luckey, 1968: Optical sphere paint and a working standard of reflectance. *Appl. Opt.*, **7**, 2289–2294.

Hale, G. M., and M. R. Querry, 1973: Optical constants of water in the 200 nm to 200 μm wavelength region. *Appl. Opt.*, **12**, 555–563.

Hansen, J. E., and J. B. Pollack, 1970: Near-infrared light scattering by terrestrial clouds. *J. Atmos. Sci.*, **27**, 265–281.

—— and L. D. Travis, 1974: Light scattering in planetary atmospheres. *Space Sci. Rev.*, **16**, 527–610.

Hanson, K., 1960: Radiation measurements on the Antarctic snowfield, a preliminary report. *J. Geophys. Res.*, **65**, 935–946.

Harding, R. H., B. Golding and R. A. Morgen, 1960: Optics of light-scattering films. Study of effects of pigment size and concentration. *J. Opt. Soc. Amer.*, **50**, 446–455.

Havens, J. M., 1964: Meteorology and heat balance of the accumulation area, McGill Ice Cap. Axel Heiberg Island Research Reports, Meteorology, No. 2, McGill University, 87 pp.

Heller, W., 1945: The determination of refractive indices of colloidal particles by means of a new mixture rule or from measurements of light scattering. *Phys. Rev.*, **68**, 5–10.

Hiltner, P. A., and I. M. Krieger, 1969: Diffraction of light by ordered suspensions. *J. Phys. Chem.*, **73**, 2386–2389.

Hobbs, P. V., 1974: *Ice Physics*. Oxford, Clarendon Press, 837 pp.

Holmgren, B., 1971: *Climate and Energy Exchange on a Subpolar Ice Cap in Summer*. Part E, Radiation Climate.

Uppsala, Meteorologiska Institutionen Uppsala Universitet, 111 pp.

Hottel, H. C., A. F. Sarofim, W. H. Dalzell and I. A. Vasalos, 1971: Optical properties of coatings: Effect of pigment concentration. *AIAA J.*, **9**, 1895–1898.

Hubley, R. C., 1955: Measurements of diurnal variations in snow albedo on Lemon Creek Glacier, Alaska. *J. Glaciol.*, **2**, 560–563.

Irvine, W. M., and J. B. Pollack, 1968: Infrared optical properties of water and ice spheres. *Icarus*, **8**, 324–360.

Joseph, J. H., W. J. Wiscombe and J. A. Weinman, 1976: The delta-Eddington approximation for radiative flux transfer. *J. Atmos. Sci.*, **33**, 2452–2459.

Kalitin, N. N., 1936: The transparency of ice to ultraviolet solar radiation. *Arktic. Inst. Tr.*, **89**, 55–70 [English translation available from Office of Technical Services, U.S. Department of Commerce, Washington, DC].

Kislovskii, L. D., 1959: Optical characteristics of water and ice in the infrared and radiowave region of the spectrum. *Opt. Spektros.* (English edition), **7**, 201–206.

Kondratiev, K. Ya., Z. F. Miranova and A. N. Otto, 1964: Spectral albedo of natural surfaces. *Pure Appl. Geophys.*, **59**, 207–216.

Kuhn, M., and L. Siogas, 1978: Spectroscopic studies at McMurdo, South Pole and Siple Stations during the austral summer 1977–78. *Antarctic J. U.S.*, **13**, 178–179.

Kukla, G. J., and H. J. Kukla, 1974: Increased surface albedo in the northern hemisphere. *Science*, **189**, 709–714.

LaChapelle, E. R., 1969: *Field Guide to Snow Crystals*. University of Washington Press, 101 pp.

Langleben, M. P., 1968: Albedo measurements of an arctic ice cover from high towers. *J. Glaciol.*, **7**, 289–297.

Liljequist, G. H., 1956: Energy exchange of an Antarctic snowfield. Short-wave radiation (Maudheim, 71°03′S, 10°56′W). *Norwegian-British-Swedish Antarctic Expedition, 1949–52, Scientific Results*, Vol. 2, Pt. 1A, Oslo, Norsk Polarinstitutt, 107 pp.

Luck, W., 1963: Beitrag zur Association des flussigen Wassers. I. *Ber. Bunsengesell. Phys. Chem.*, **67**, 186–190.

Lyons, J. B., and R. E. Stoiber, 1959: The absorptivity of ice: A critical review. Sci. Rep. No. 3, Dartmouth College, 13 pp.

Mellor, M., 1977: Engineering properties of snow. *J. Glaciol.*, **19**, 15–66.

Middleton, W. E. K., and A. G. Mungall, 1952: The luminous directional reflectance of snow. *J. Opt. Soc. Amer.*, **42**, 572–579.

Mugnai, A., and W. J. Wiscombe, 1980: Scattering of radiation by moderately nonspherical particles. *J. Atmos. Sci.*, **37**, 1291–1307.

Nakaya, V., 1954: *Snow Crystals: Natural and Artificial*. Harvard University Press, 510 pp.

Ockman, N., 1958: The infrared and Raman spectra of ice. *Advances in Physics*, Vol. 7, Academic Press, 199–220.

Palmer, K. F., and D. Williams, 1974: Optical properties of water in the near infrared. *J. Opt. Soc. Amer.*, **64**, 1107–1110.

Patel, C. K. N., and A. C. Tam, 1979: Optical absorption coefficients of water. *Nature*, **280**, 302–304.

Paterson, W. S. B., 1969: *The Physics of Glaciers*. Pergamon Press, 250 pp.

Patterson, E. M., C. E. Shelden and B. H. Stockton, 1977: Kubelka-Munk optical properties of a barium sulfate white reflectance standard. *Appl. Opt.*, **16**, 729–732.

Petzold, D. E., 1977: An estimation technique for snow surface albedo. *Clim. Bull.* (McGill University), **21**, 1–11.

Pollack, J. B., and J. N. Cuzzi, 1980: Scattering by nonspherical particles of size comparable to a wavelength: A new semi-empirical theory and its application to tropospheric aerosols. *J. Atmos. Sci.*, **37**, 868–881.

Post, A., and E. R. LaChapelle, 1971: *Glacier Ice*. University of Washington Press, 110 pp.

Reding, F. P., 1951: The vibrational spectrum and structure of several molecular crystals at low temperature. Ph.D. thesis, Brown University, 147 pp.

Roulet, R. R., G. A. Maykut and T. C. Grenfell, 1974: Spectrophotometers for the measurement of light in polar ice and snow. *Appl. Opt.*, **13**, 1652–1658.

Rusin, N. P., 1961: *Meteorologicheskiy i radiatsionyy rezhim Antarktidy*. Leningrad, Gidrometeorologischeskoye Izdatel'stvo. [English translation: *Meteorological and Radiational Regime of Antarctica*. Jerusalem, Israel Program for Scientific Translations, 1964, 355 pp.].

Sarofim, A. F., H. C. Hottel and E. J. Fahimian, 1968: Scattering of radiation by particle layers. *AIAA J.*, **6**, 2262–2266.

Sauberer, F., 1938: Versuche uber spectrale Messungen der Strahlungseigenschaften von Schnee und Eis mit Photoelementen. *Meteor. Z.*, **55**, 250–255.

——, 1950: Die spektrale Strahlungsdurchlässigkeit des Eises. *Wetter und Leben*, **2**, 193–197.

Schaaf, J. W., and D. Williams, 1973: Optical constants of ice in the infrared. *J. Opt. Soc. Amer.*, **63**, 726–732.

Schlatter, T. W., 1972: The local surface energy balance and subsurface temperature regime in Antarctica. *J. Appl. Meteor.*, **11**, 1048–1062.

Schwerdtfeger, P., 1969: Absorption, scattering and extinction of light in ice and snow. *Nature*, **222**, 378–379.

Siegel, R., and J. R. Howell, 1972: *Thermal Radiation Heat Transfer*. McGraw-Hill, 814 pp.

Sommerfeld, R. A. and E. LaChapelle, 1970: The classification of snow metamorphism. *J. Glaciol.*, **9**, 3–17.

Stephenson, P. J., 1967: Some considerations of snow metamorphism in the Antarctic ice sheet in the light of ice crystal studies. *Physics of Snow and Ice*, H. Oura, Ed., *Proc. Int. Conf. Low Temperature Sciences*, 14–19 August 1966, Sapporo, Japan, Bunyeido Printing Company, 725–740.

Strong, A. E., E. P. McClain and D. F. McGinnis, 1971: Detection of thawing snow and ice packs through the combined use of visible and near-infrared measurements from earth satellites. *Mon. Wea. Rev.*, **99**, 828–830.

Tam, A. C., and C. K. N. Patel, 1979: Optical absorptions of light and heavy water by laser optoacoustic spectroscopy. *Appl. Opt.*, **18**, 3348–3358.

van de Hulst, H. C., 1957: *Light Scattering by Small Particles*. Wiley, 470 pp.

Vedernikova, E. A., and M. V. Kabanov, 1974: Scattering of optical radiation by a system of closely spaced scatterers. *Opt. Spectrosc.*, **37**, 71–74.

Warren, S. G., and W. J. Wiscombe, 1980: A model for the spectral albedo of snow. II. Snow containing atmospheric aerosols. *J. Atmos. Sci.*, **37**, 2734–2745.

Weller, G., 1968: Heat-energy transfer through a four-layer system: Air, snow, sea ice, sea water. *J. Geophys. Res.*, **73**, 1209–1220.

——, 1969: Radiation diffusion in Antarctic ice media. *Nature*, **221**, 355–356.

Wiscombe, W. J., 1977: The Delta-Eddington approximation for a vertically inhomogeneous atmosphere. NCAR Tech. Note 121 [NTIS P6270618].

——, 1979: Mie scattering calculations: Advances in technique and fast, vector-speed computer codes. NCAR Tech. Note TN-140+STR [NTIS PB 301388].

——, 1980: Improved Mie scattering algorithms. *Appl. Opt.*, **19**, 1505–1509.

——, and J. H. Joseph, 1977: The range of validity of the Eddington approximation. *Icarus*, **32**, 362–377.

Zerull, R. H., 1976: Scattering measurements of dielectric and absorbing nonspherical particles. *Beitr. Phys. Atmos.*, **49**, 166–168.

Reprinted from JOURNAL OF THE ATMOSPHERIC SCIENCES, Vol. 37, No. 12, December 1980
American Meteorological Society
Printed in U. S. A.

A Model for the Spectral Albedo of Snow. II: Snow Containing Atmospheric Aerosols

STEPHEN G. WARREN[1] AND WARREN J. WISCOMBE

National Center for Atmospheric Research,[2] Boulder, CO 80307

(Manuscript received 15 April 1980, in final form 28 August 1980)

ABSTRACT

Small highly absorbing particles, present in concentrations of only 1 part per million by weight (ppmw) or less, can lower snow albedo in the visible by 5–15% from the high values (96–99%) predicted for pure snow in Part I. These particles have, however, no effect on snow albedo beyond 0.9 μm wavelength where ice itself becomes a strong absorber. Thus we have an attractive explanation for the discrepancy between theory and observation described in Part I, a discrepancy which seemingly cannot be resolved on the basis of near-field scattering and nonsphericity effects.

Desert dust and carbon soot are the most likely contaminants. But careful measurements of spectral snow albedo in the Arctic and Antarctic point to a "grey" absorber, one whose imaginary refractive index is nearly constant across the visible spectrum. Thus carbon soot, rather than the red iron oxide normally present in desert dust, is strongly indicated at these sites. Soot particles of radius 0.1 μm, in concentrations of only 0.3 ppmw, can explain the albedo measurements of Grenfell and Maykut on Arctic Ice Island T-3. This amount is consistent with some observations of soot in Arctic air masses. 1.5 ppmw of soot is required to explain the Antarctic observations of Kuhn and Siogas, which seemed an unrealistically large amount for the earth's most unpolluted continent until we learned that burning of camp heating fuel and aircraft exhaust indeed had contaminated the measurement site with soot.

Midlatitude snowfields are likely to contain larger absolute amounts of soot and dust than their polar counterparts, but the snowfall is also much larger, so that the ppmw contamination does not differ drastically until melting begins. Nevertheless, the variations in absorbing particle concentration which *will* exist can help to explain the wide range of visible snow albedos reported in the literature.

Longwave emissivity of snow is unaltered by its soot and dust content. Thus the depression of snow albedo in the visible is a systematic effect and always results in more energy being absorbed at a snow-covered surface than would be the case for pure snow. Thus man-made carbon soot aerosol may continue to exert a significant warming effect on the earth's climate even after it is removed from the atmosphere.

1. Introduction

In Part I of this paper (Wiscombe and Warren, 1980) a model for calculating snow spectral albedo was presented. The comparison of its results with observations showed good agreement in the near-infrared (near-IR), where the reduction in snow albedo with age could be mimicked by reasonable increases in snow grain size (Part I, Figs. 10 and 15). For the visible wavelengths, however, where the albedo is highest, the model consistently calculated albedos higher than are normally observed. The discrepancy is greater for melting snow than for new snow.

Fig. 1 illustrates the problem we are confronting. The solid line is a recent measurement of spectral albedo at South Pole Station by Kuhn and Siogas (1978). In order for our model predictions (the small circles) to match these observations in the near-IR ($0.9 \leq \lambda \leq 1.5$ μm) we require a snow grain radius $r = 100$ μm, which is reasonable for the surface of the Antarctic plateau (Stephenson, 1967). But using this grain radius at shorter wavelengths results in albedos up to 10% higher than observed. A larger grain size would reduce the albedo at *all* wavelengths, thus destroying our good agreement in the near-IR.

The probable presence of absorbing impurities in the snow provides a way out of this dilemma. Because ice is so weakly absorptive in the visible region, very small amounts of dust or soot may be capable of reducing the albedo there, while having little effect in the near-IR where ice itself is highly absorptive. Our hypothesis, then, is that measured snow albedos at visible wavelengths are significantly lower than pure-snow values due to the presence of dust or soot.

Using the simple model of Part I, we show below how snow albedo depends on dust concentration, dust composition and dust particle sizes. We investigate first the effect of desert dust, which is a

[1] Present affiliation: Cooperative Institute for Research in Environmental Sciences, University of Colorado, Boulder 80309.

[2] The National Center for Atmospheric Research in sponsored by the National Science Foundation.

0022-4928/80/122734-12$07.00

mixture of materials whose aggregate optical properties have been studied, and second the effect of carbon soot alone, which may normally be the principal absorptive component of atmospheric aerosols that find their way into snow.

2. Observations relating to atmospheric aerosols in snow

Dust enters snow as ice nuclei, as particles scavenged by falling snow crystals, and by fallout. Clay mineral particles, blown up primarily from the world's deserts, form a major component of the global background aerosol (Pruppacher and Klett, 1978). These dust particles can travel thousands of kilometers to reach snow-covered regions (Prospero, 1979, and references therein).

Snow crystals are usually nucleated by micron-sized clay mineral particles, and the crystals become effective scavengers when they fall. Magono *et al.* (1979) found falling snow crystals to have collection efficiency near unity for all aerosols in the size range 0.1 to 5.0 μm. The third mechanism—fallout—is also important, at least in midlatitudes. Falconer and Hogan (1971) found much more dust in snow on the ground than they found in falling snowflakes.

The dust incorporated into snow by all three mechanisms is predominantly clay minerals, except where the marine influence is strong, e.g., over Antarctica, where sea salts tend to dominate. But we can ignore sea salts in this study because they are almost perfectly transparent at solar wavelengths (Toon *et al.*, 1976). Many of the clay minerals are also relatively transparent, but they typically have highly absorptive inclusions such as iron oxide, carbon or organic materials (Lindberg, 1975).

Kumai (1976, 1977) has identified the impurities in falling snow at Camp Century (Greenland) and at the South Pole. He typically found one large nucleus at the center and several smaller particles (presumably scavenged) elsewhere in each snow crystal. At Camp Century 84% of the nuclei were clay minerals, 10% unidentified insoluble minerals and 1% soluble sea salt (5% had no nucleus). Kumai found the bulk concentration of clay mineral particles in falling snow to be 0.034 ppmw, and most of these particles were at the centers of snow crystals. This compares with the value of 0.035 ppmw found earlier by Murozumi *et al.* (1969) and with a value of 0.050 ppmw we calculate from data of Hamilton and Langway (1967). Kumai found a size distribution somewhat resembling a Junge power law, but with a plateau around 1 μm, which is the typical average size of these particles.

At the South Pole, Kumai found considerably more soluble particles in the snow (20%) but still the majority (59%) of the nuclei were clay minerals. The total clay mineral concentration was lower than in Greenland, only 0.015 ppmw. Murozumi *et al.* (1969) obtained an even lower estimate, only 0.002 ppmw of terrestrial dust, at Byrd Station (West Antarctica) by multiplying the silicon concentration by 5.

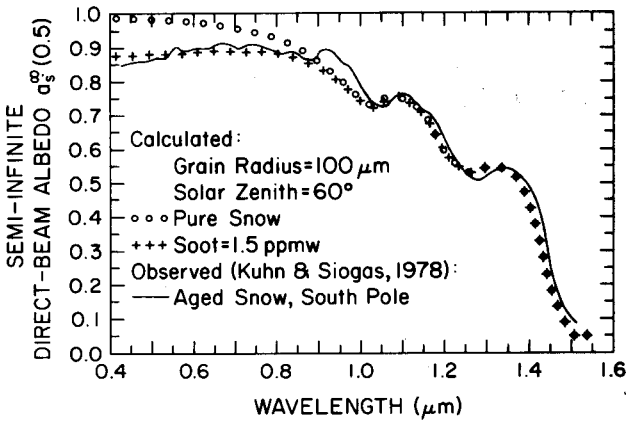

FIG. 1. Snow albedo at South Pole Station, calculation and measurement.

This enhancement of sea salt relative to continental dust, and the very low total concentrations of continental dust in Antarctic aerosol, can be attributed to the long distance from significant sources of dust in Australia and southern Africa. The frequent storms in the oceanic zone surrounding Antarctica remove much dust by rainout and washout, making Antarctic snow the cleanest on earth.

These dust concentrations in falling snow are usually preserved if there is no melting. Dust is found in all polar ice cores (Thompson, 1977; Hammer, 1977; Koerner, 1977). Dust has been used to identify annual layers even at locations where snowmelt does not occur, because a maximum is found every spring at some locations (Langway *et al.*, 1977; Hammer, 1977).

Dust layers are found in temperate glaciers (Post and LaChapelle, 1971, Figs. 6–11) corresponding to the summer melt season. This may be due to clay-mineral dust accumulating at the surface instead of percolating down with the meltwater, or to dry fallout during the time of no snowfall (Kohno and Maeno, 1979). Dust concentrations measured in these dirty layers presumably are representative of the end of the melt season. For example, Koerner (1977, Fig. 3) shows concentrations of dust in the annual dirty layers of an ice core on Devon Island to be 5–10 times as high as concentrations in the intervening clean layers. The top of Devon Island undergoes a short melt season (July only), so the concentrating of dust would presumably be larger where the melt season is longer.

At lower latitudes we might expect considerably

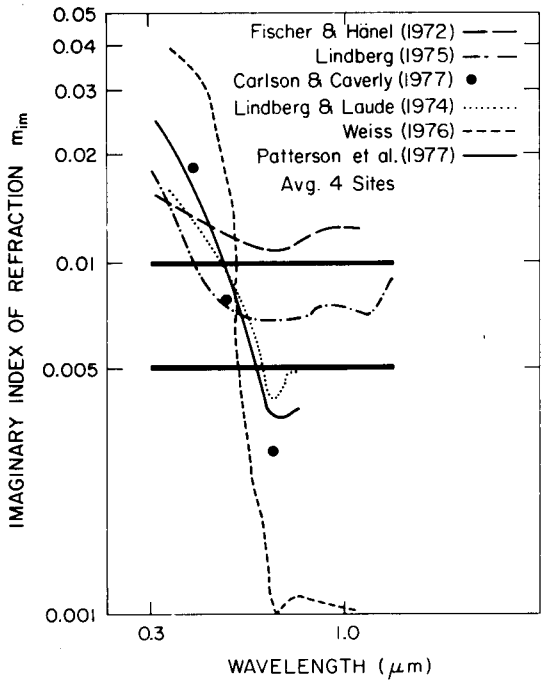

FIG. 2. Imaginary index of refraction for desert dust as a function of wavelength from various sources; taken from Carlson and Benjamin (1980, Fig. 3).

higher dust concentrations than those cited above. Dust concentrations in the surface layer of a perennial mountain snowfield in Japan during the melt season were reported by Higuchi and Nagoshi (1977), who simultaneously measured total albedo. The average dust concentration between 30 and 300 cm below the surface was 5 ppmw at the beginning of the melt season; i.e., this "clean" snow already contained 100 times the dust concentration found on the Greenland and Antarctic plateaus. As the summer progressed, the particulate matter was found to be retained in the topmost 1 cm. The dust concentration in this topmost centimeter at the beginning of the melt season (June) was already 100 ppm. The spectrally-integrated albedo was observed to drop from 60% (for 100 ppm dust) to 15% (for 4000 ppm dust).

For the Quelccaya Ice Cap at 14°S in the Andes (Thompson *et al.*, 1979), the average dust concentration was 5 ppm for snow 4.5–5.5 m below the surface. The dirtiest sample contained 8.8 ppmw dust, whereas the cleanest contained 1.2 ppmw. These concentrations are two orders of magnitude greater than those found in Antarctic snow, but close to those found by Higuchi and Nagoshi (1977) in Japan. The dust particle size distribution for Quelccaya has an effective mean radius (for snow albedo purposes) of about $r = 1.3$ μm.

Optical properties of desert dust have been reviewed by Lindberg (1975) and by Carlson and Benjamin (1980). We reproduce Carlson and Benjamin's compilation of the imaginary refractive index in Fig. 2. The measurements of Lindberg and his coworkers were for desert dust collected in southern New Mexico. Most of the others were for dust which blew off the Sahara over the North Atlantic. There are considerable differences among the various investigations. Patterson *et al.* (1977) reported good agreement for m_{im} among samples collected at four locations spaced across the Atlantic in 1974. Their results show a strong decrease of m_{im} between 0.3 and 0.7 μm wavelength (which would make the dust appear red), but others (in particular Fischer and Hänel, 1972) show m_{im} more nearly constant with wavelength. In the remainder of this paper we use the term "red dust" to refer to dust whose $m_{im}(\lambda)$ is that reported by Patterson *et al.* (1977).

The measured values of m_{im} in the visible region are of the order of 10^{-2}. These values are not characteristic of any pure substance commonly found in soil. Clay minerals have $m_{im} \leq 10^{-4}$ (Lindberg, 1975), while highly absorptive substances like Fe_3O_4 (Becquerel and Rossignol, 1929) or graphitic carbon (Twitty and Weinman, 1971) have $m_{im} \approx 1$; only some volcanic minerals have $10^{-4} < m_{im} < 10^{-1}$ (Pollack *et al.*, 1973). Microscopic investigations indicate that the small highly-absorptive particles stick on to the large clay particles to create a sort of raisin-pudding effect (Lindberg, 1975). Thus the measurements of m_{im} for continental dust represent some sort of average.

The differences in Fig. 2 are probably attributable to variability in dust composition. An abundance of iron oxide would explain the "red dust" curves. The wavelength dependence of m_{im} becomes less steep if the dust contains a grey absorber like graphitic carbon. Lindberg (1975) attempted to match the optical properties of natural New Mexico dust by preparing a synthetic mixture of clay minerals. The synthetic mixture had higher diffuse reflectance at all wavelengths out to 2.5 μm, and steeper wavelength dependence in the visible, than did the natural dust. But, by adding 0.5% by weight of carbon soot to the synthetic mixture, Lindberg was able to match the natural dust reflectance. This suggests that variable soot content may be responsible for many of the differences between measurements in Fig. 2.

Rosen *et al.* (1978) have used Raman spectroscopy to identify the absorbing component in urban aerosols as graphitic carbon. It also has been shown to be the dominant absorber in aerosols collected in rural regions of the United States (Weiss *et al.*, 1979). Graphitic carbon aerosol particles are produced by incomplete combustion in forest fires, brush fires, and industrial furnaces and engines. Seiler and Crutzen (1980) estimate that both natural and industrial sources are of comparable magnitude at present.

Graphitic carbon soot consists of randomly oriented graphite crystallites ($r \approx 20$ Å) embedded in a matrix of amorphous carbon (Franklin, 1950; 1951). Single crystals of pure graphite are highly birefringent, with both m_{re} and m_{im} depending on crystal orientation (Greenaway *et al.*, 1969), but the random arrangement of these crystals in soot means that soot particles will not exhibit optical anisotropy. Soot is generally not pure carbon. The complex refractive index varies as the *C/H* ratio varies, with m_{im} generally increasing with increasing carbon content (McCartney *et al.*, 1965; Foster and Howarth, 1968; Dalzell and Sarofim, 1969). Because of this, the measured values of $m_{im}(\lambda)$ show some spread, but they generally agree that m_{im} is independent of λ, to within a factor of 2, for $0.3 \leq \lambda \leq 0.9\ \mu$m. Dalzell and Sarofim (1969, Table 1) found, for both acetylene soot and propane soot, $m \approx 1.6 - 0.5i$, essentially independent of wavelength in the visible spectrum. Twitty and Weinman (1971) reviewed some other measurements of m for carbonaceous materials and chose for their calculation a median value (constant with wavelength) $m = 1.8 - 0.5i$. Since we lack exact knowledge of the source and *C/H* ratio of the graphitic carbon that may be present in snow, we will use the latter value in our calculations below.

There are observations which indicate the efficacy of small particles in reducing snow albedo. Liljequist (1956) noted that in an area downwind from the hut at Maudheim, where soot particles fell out, snowmelt was dramatically accelerated, while elsewhere the snow remained dry. Hanson (1960) also reported reduced snow albedo due to dust or soot from human habitation at an Antarctic station. Dunne and Price (1975) reported that in Labrador aerosol pollution from a small town drops snow albedo down to 50% or less within a few days after each snowfall.

When dust or soot concentrations are very large, the effect on snow albedo can be seen by the naked eye. Elgmork *et al.* (1973) show a photograph of stratigraphy in winter snow in southern Norway. Distinct grey bands suggest episodic pollution events involving soot. Episodic red or yellow snow has also been reported, in conjunction with dust storms in regions adjacent to deserts. Red dust in Alpine snow comes from the Sahara (reviewed by Haeberli, 1977); in New Zealand snow, from Australia (Marshall and Kidson, 1929); in the Tien Shan, from Central Asian deserts (Khromov, 1931; Glazovskaya, 1954); and in the eastern United States, from the American desert and "dust bowl" (Byers, 1936; Robinson, 1936). (Photosynthetic algae growing in melting snow can also give it a red color, but in the examples cited here it was dust rather than algae that produced the color.)

3. Albedo of snow containing desert dust

We shall assume that desert dust is distributed uniformly through a snowpack as spheres with given radii and of density 2.4 g cm^{-3}. The real index of refraction for clay-mineral dust is ~1.55 (Carlson and Benjamin, 1980) and we take it to be constant at this value for all wavelengths.

With these assumptions, there remain three dust parameters which affect snow albedo: concentration, mean size, and spectral imaginary refractive index. Mie calculations are done separately for the dust particles and the ice particles and averaged using the respective cross-sectional areas per unit volume as weight factors. The resulting single-scattering coalbedo ($1 - \tilde{\omega}$) is shown in Fig. 3a for a snow grain radius $r_{ice} = 1000\ \mu$m, a dust particle mean radius $r_{dust} = 1\ \mu$m, and a "red dust" imaginary index m_{im}(dust). [For $\lambda > 0.7\ \mu$m, m_{im}(dust) is assumed constant and equal to its value at $\lambda = 0.7\ \mu$m.] The dust raises ($1 - \tilde{\omega}$) significantly for $\lambda < 0.9\ \mu$m, where $m_{im}(\text{dust}) \gg m_{im}(\text{ice})$. At longer wavelengths, dust concentrations up to 100 ppmw have almost no effect on $\tilde{\omega}$ because ice is more absorptive and it swamps the dust effect by virtue of its much larger volume fraction. This is consistent with the observation by Dirmhirn (1960) that an episode of yellow Saharan dust falling into Alpine snow reduced the visible albedo more than it reduced the spectrally integrated albedo (16 and 10% reduction, respectively).

Fig. 4a shows diffuse snow albedo (a_d^∞) versus wavelength for 20 ppmw of red dust embedded in snow with grain radii of 1 mm. For fixed concentration, smaller dust particles are always more effective in lowering the albedo than larger ones. The snow would appear grey for 10 μm dust particles, but for particles $\leq 1\ \mu$m a pronounced albedo peak in the red appears, in agreement with certain observations quoted earlier.

Albedos calculated using Kumai's (1977) size distribution for dust in Greenland snow, even when it was extrapolated to include even larger particles, were barely distinguishable from our $r_{dust} = 1\ \mu$m results in Fig. 4a. The same is true for the particle size distributions measured in both dirty and clean layers of the tropical Quelccaya Ice Cap (elevation 5650 m).

The mean particle size may be larger at lower elevations and nearer to sources. Higuchi and Nagoshi (1977) found the most frequently occurring radius to be 2–5 μm, depending on season, on a mountain snowfield in Japan. Windom (1969) reported size distributions for various minerals from a variety of midlatitude mountain snowfields. The peaks were near $r = 1\ \mu$m for St. Elias snowfields (Alaska/Yukon) but larger, up to $r = 10\ \mu$m, for snowfields in New Zealand, Mexico and Mt. Olym-

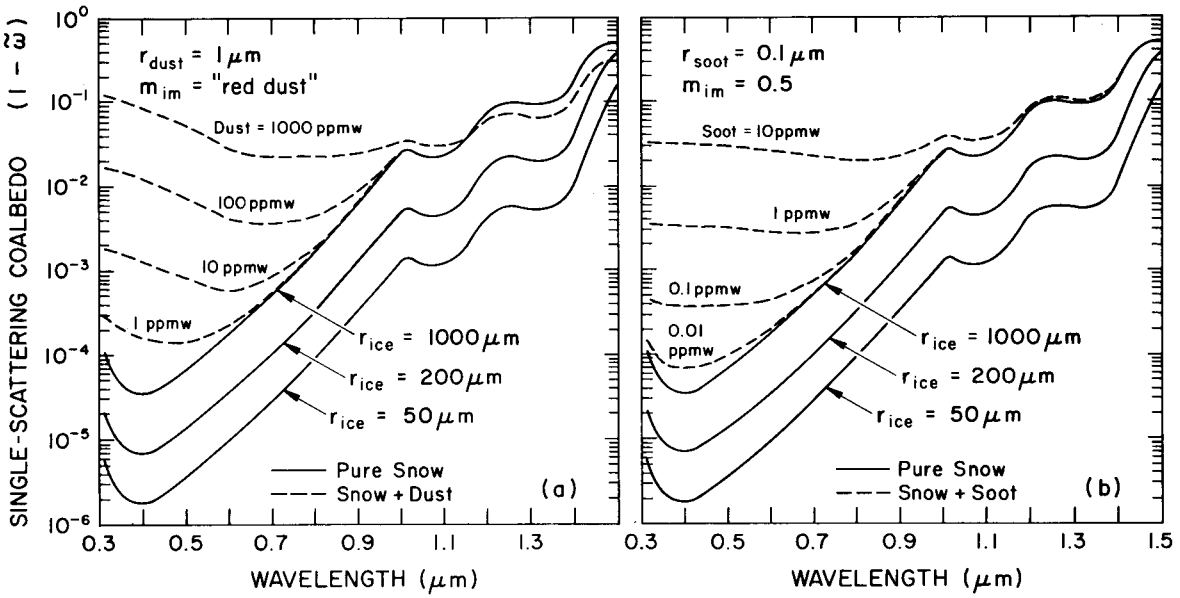

FIG. 3. Effect of solid impurities on single-scattering coalbedo ($1 - \tilde{\omega}$). Solid lines are taken from Fig. 3a of Part I. Dashed lines show the effect of adding (a) dust or (b) soot in various concentrations to ice spheres of radius 1000 μm.

pus (Washington). However, Patterson and Gillette (1977) found the mean radius for soil-derived aerosols to be 1.5 μm, even at low-elevation continental locations.

Fig. 5 shows albedo calculations for snow containing dust particles of radii 1 μm (Figs. 5a and 5c) and 5 μm (Figs. 5b and 5d). The incident radiation is a direct beam at solar zenith angle $\theta = 60°$; the results for incident diffuse radiation would be very similar (cf. Part I, Section 5b). We consider 1 μm dust particles to be more typical for large snowfields, polar ice caps and snow-covered sea ice, but 5 μm particles may be characteristic of snow very near to sources of dust. In each case we have plotted our calculated spectral albedo for pure snow and for snow containing dust in concentrations from 1 to 1000 ppmw. Only albedos for $\lambda < 1.5$ μm are shown because for longer wavelengths the dust effect is negligible. Note, however, that for *very* dirty snow (1000 ppmw of dust in Fig. 5c) the albedo for $\lambda > 1$ μm is substantially *increased* in the case of fine dust in coarse snow.

For each dust concentration, the albedo in Fig. 5 is plotted using three different spectral imaginary index cases: constant values of 0.005 and 0.01 (the two thick lines in Fig. 2) and the measured values for red dust of Patterson *et al.* (thin solid line in Fig. 2). Calculations using the spectral m_{im}(dust) of Fischer and Hänel (1972) (shown in Fig. 2) produced results nearly indistinguishable from the case of m_{im}(dust) = 0.01. The values 0.005 and 0.01 represent reasonable bounds on the measured values of "average imaginary index" (see, e.g., Lindberg, 1975).

The two constant imaginary index cases have essentially similar effects on the snow albedo. They tend to make it a much flatter function of wavelength between 0.3 and 0.8 μm than it was without dust, a phenomenon which is similar to the effect of small depth (Fig. 13 of Part I). By contrast, the Patterson imaginary index leads to a very strong wavelength dependence as dust concentration increases, with the visible peak displaced to larger and larger wavelengths. This is especially true for the more realistic case $r_{dust} = 1$ μm (Figs. 5a and 5c).

The upper frames in Fig. 5 are for $r_{ice} = 100$ μm (new snow); the lower for $r_{ice} = 1000$ μm (old melting snow). For the *same* dust concentration, the albedo is reduced more for $r_{ice} = 1000$ μm than for $r_{ice} = 100$ μm. This is because the radiation penetrates deeper in more coarsely grained snow and encounters more absorbing material before it can reemerge from the snowpack.

We now attempt to match snow albedo measurements from the central Arctic Ocean by calculating the albedo of snow containing desert dust. In Fig. 6a we take the dust size to be $r = 1$ μm, and its imaginary index that of "red dust." The observations of Grenfell and Maykut (1977) are plotted as solid lines only out to $\lambda = 0.9$ μm, because for $\lambda > 0.9$ μm the spectral resolution is poor (Grenfell, personal communication). In order of decreasing albedo, the three curves are for dry cold snow, wet new snow, and old melting snow. The snow grain size was chosen in each case as that which produced agreement between calculated and observed albedo at $\lambda = 0.9$ μm for pure snow, since at this wavelength dust has negligible effect on albedo. The grain sizes were thus

chosen to be r = 110, 300 and 1300 μm, respectively. When these grain sizes are used to calculate albedo for shorter wavelengths, the results for pure snow (circles) exceed the observations.

In order to reduce these calculated values to the observed levels, 10–15 ppmw of dust was required (plus signs in Fig. 6a). The calculated albedo, however, shows a strong spectral variation. If this type of dust were present in snow, the snow would appear red or orange, with a peak in albedo at $\lambda \approx 0.6$ μm. This is clearly not observed for the snow albedo in the central Arctic but may be true for snow in regions closer to deserts. The dotted lines in Fig. 5c show that the wavelength of maximum albedo decreases as the dust concentration is reduced. Thus, the reports of red or yellow snow mentioned above may owe their variability in color to a variability in dust concentration. The dust is normally reported to be red as it falls (Haeberli, 1977), but can appear yellow when diluted in snow. In a firn-core in the high Alps (Oeschger *et al.*, 1977), the snow tentatively assigned to the time of the 1936–37 dustfalls was yellow.

If dust is responsible for the low observed snow albedo at Arctic Ice Island T-3, its m_{im} apparently cannot be that of red dust. If we use the m_{im} obtained for Saharan dust by Fischer and Hänel (1972) or a flat $m_{\text{im}} = 0.005$ independent of wavelength, we obtain rather better agreement with observation. Fig. 6b shows that 13–20 ppm of dust ($m_{\text{im}} = 0.005$) can account for the albedo observations at T-3. However, it is unlikely that this amount of dust is present in Arctic snow. Mullen *et al.* (1972) and Darby *et al.* (1974) reported only 1 ppmw dust in snow at T-3.

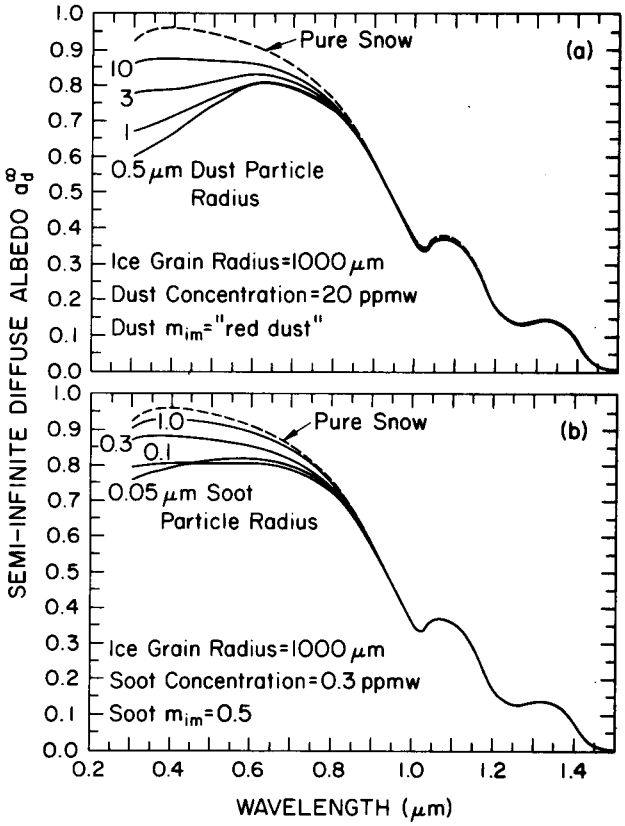

FIG. 4. Effect of (a) dust or (b) soot particle size on snow albedo a_d^s.

4. Albedo of snow containing carbon soot

In order to explain the Grenfell and Maykut albedo measurements, we apparently need more dust than is observed, if we use m_{im}(dust) = 0.005. But, as pointed out above, $m_{\text{im}} = 0.005$ is not characteristic of any pure substance. In fact, the components of natural dust have highly contrasting imaginary indices and different size distributions. For New Mexico dust, Gillespie *et al.* (1978) did separate Mie calculations for the small-sized absorbing component (carbon) and the large-sized relatively transparent components and averaged the results. Compared to Mie quantities obtained using the "average" m_{im}, there were often large differences. In particular, the single-scattering albedo fell dramatically when the two components were treated separately. Mita and Isono (1980) also showed how, for the same weight-fractions of the two components, different size distributions of the absorptive component led to different "average" m_{im} values.

We saw that we could only match the Arctic snow albedo observations by the use of an m_{im} for dust that was fairly constant with wavelength (Fig. 6b). If the "average" m_{im} of dust is independent of wavelength, the absorptive component is most likely carbon. So we follow the example of Gillespie *et al.* and do Mie calculations for the carbon particles by themselves, ignoring the relatively transparent particles which are unimportant for snow albedo.

We assume soot is present in the snow as small particles of radius 0.1 μm, density[3] 2.05 g cm^{-3}, and refractive index $m = 1.8 - 0.5i$ (Twitty and Weinman, 1971). Fig. 3b shows the effect of soot on the single-scattering albedo of coarse-grained snow (r = 1000 μm). Comparison with Fig. 3a shows 1) the effect of 1 ppm of soot is as large as the effect of 100 ppm of dust; 2) soot affects $\tilde{\omega}$ only at the short

[3] (Note added in revision.) This density would be typical of a mixture of graphite and amorphous carbon. Together with the given values of r and m, it implies an absorption cross section at visible wavelengths of 3.7 m^2 g^{-1} (blue) to 5.7 m^2 g^{-1} (red). However, the individual 0.1 μm size soot particles may themselves contain gaseous inclusions, so that a more realistic density might be 1 g cm^{-3} (Rosen, personal communication), implying a visible absorption cross section of 7.4–11.5 m^2 g^{-1}. If so, the reduction of snow albedo which we show for a given soot concentration should actually be attributed to half that concentration.

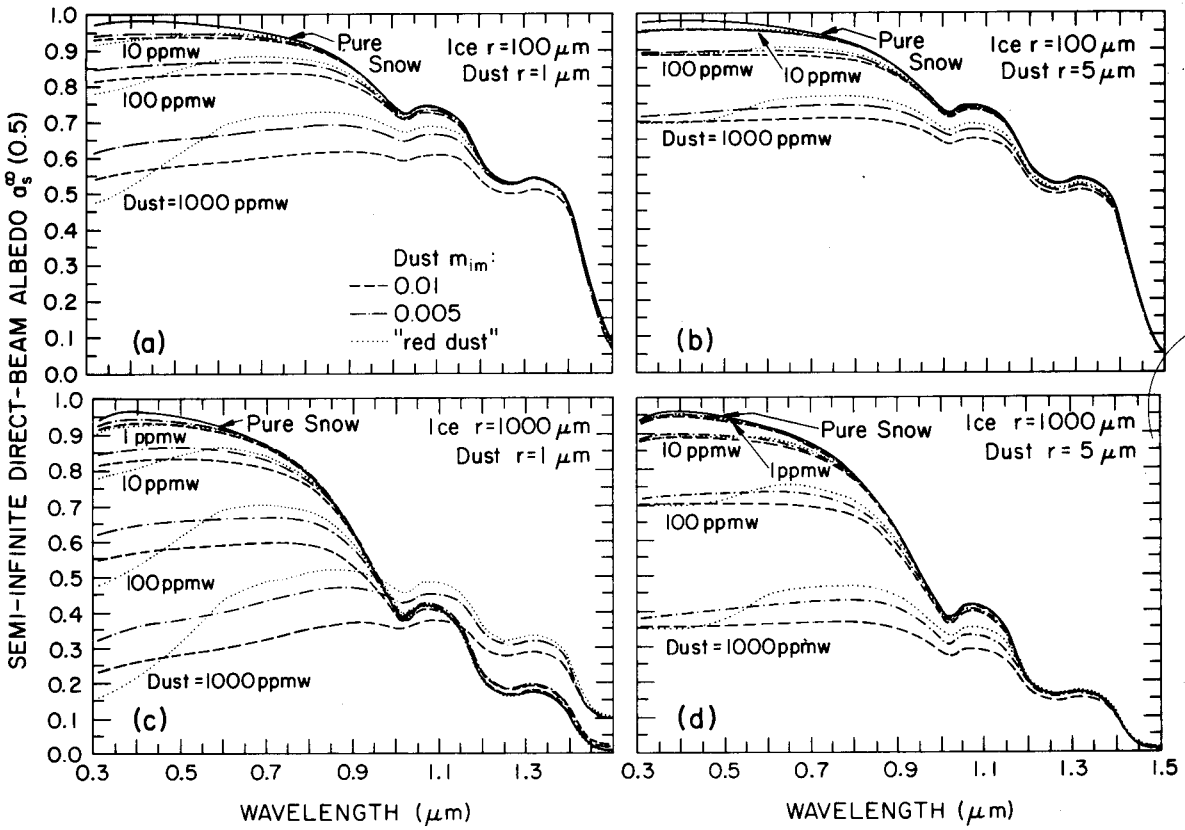

FIG. 5. Effect of snow and dust parameters on albedo a_s^∞ ($\mu_0 = 0.5$). The four frames are for different combinations of dust particle radius and snow grain radius. In each frame, results are shown for several dust concentrations. For each dust concentration, the albedo is plotted for three different $m_{im}(\lambda)$.

wavelengths (just as for dust); and 3) 1 ppm soot results in $(1 - \tilde{\omega})$ rather constant with wavelength in the visible, whereas 100 ppm "red dust" gave a minimum at wavelength 0.6–0.7 μm.

The effect of soot particle radius on snow albedo is shown in Fig. 4b, for coarse-grained snow and a soot concentration of 0.3 ppmw. As for dust (Fig. 4a), the albedo drops as the soot particle size decreases. Twitty and Weinman (1971) suggested a model size distribution for soot particles which was based on observations of urban air by Peterson *et al.* (1969). When we used this distribution, we obtained the same spectral snow albedo as for the monodisperse $r = 0.1$ μm case in Fig. 4b. Therefore, in all the calculations below which include soot we have used r(soot) = 0.1 μm. [Recently, Whitby (1979, Fig. 4) reported a bimodal size distribution, a "nuclei mode" at $r = 0.015$ μm and an "accumulation mode" at $r = 0.1$ μm. As explained by Weiss *et al.* (1979, Fig. 2) and Bergstrom (1979, Fig. 1), this distribution should have the same absorption coefficient per unit mass as the monodisperse $r = 0.1$ μm soot we are using.]

The effect of soot concentration on direct-beam ($\theta = 60°$) snow albedo is shown in Fig. 7 for two different snow grain sizes. As with dust (Fig. 5), a particular concentration of soot is calculated to have much more effect on the albedo of old melting snow ($r = 1000$ μm) than on that of new snow ($r = 100$ μm).

The darkened snow is calculated to be essentially grey in the visible, in contrast to the strong peak in the red for red dust. A weight fraction of 10^{-7} for soot in snow ($r = 1000$ μm) is calculated to reduce the albedo at $\lambda = 0.4$ μm by 7%. Even a weight fraction as low as 10^{-8} is calculated to reduce the albedo at this wavelength by 1%.

Fig. 6c shows that a soot concentration of 0.3–0.4 ppmw is required in our model to match the albedo observations of Grenfell and Maykut (1977). There are some discrepancies in exact shape between the two curves; they could be explained if the soot in the Arctic snow were found to have an m_{im} increasing slightly with wavelength instead of constant as we have assumed.

Measurements have not been published of concentrations of graphitic carbon in snow. If we accept Mullen *et al.*'s (1972) report of 1 ppm dust in snow at T-3, we are forced to hypothesize that 30–40% of the total dust is present as soot. This would not be unusual for an industrial city, but seems high for a remote area. However, the air in the high Arctic is often visibly polluted, most likely

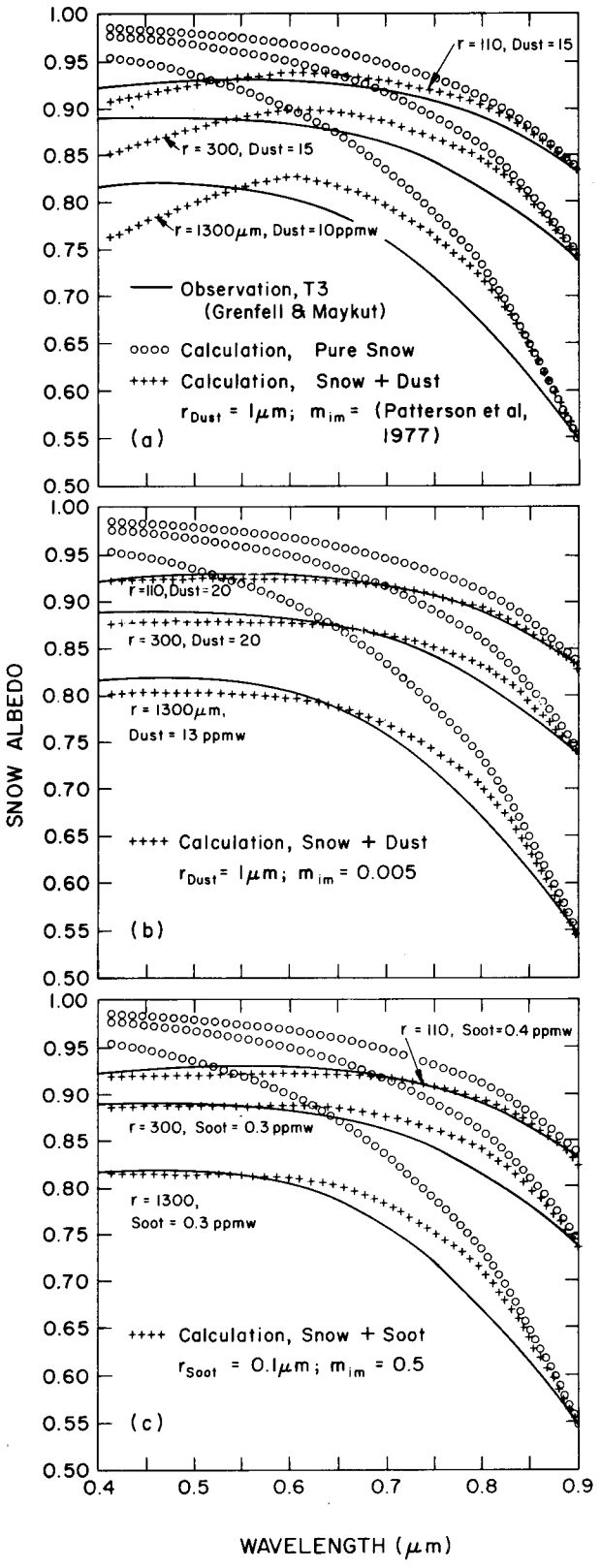

FIG. 6. Comparison of calculated snow albedo a_d^∞ with observations. (a), (b) and (c) are identical except for the plus-sign curves which refer to different types of snow contamination.

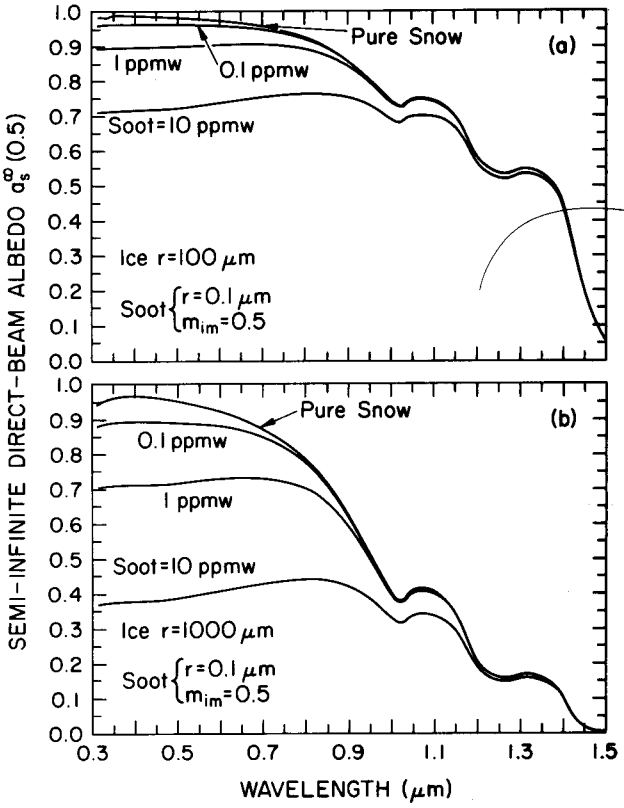

FIG. 7. Effect of soot concentration on albedo a_s^∞ ($\mu_0 = 0.5$). (a) $r_{ice} = 100$ μm, (b) $r_{ice} = 1000$ μm.

from industrial sources in Europe (Rahn and McCaffrey, 1979; Rahn, personal communication). The concentrations of trace elements in the atmosphere at Barrow (Rahn and McCaffrey, 1979) are 4 to 10 times as high as in Greenland (Herron *et al.*, 1977) or in the Antarctic (Boutron and Lorius, 1979). The concentration of soot in air arriving at Barrow from the north ("the clean air sector") is as much as one-tenth of that in the air in New York City (Rosen, personal communication). Rahn (personal communication) estimates that soot would be present in Arctic snow at a level of 0.2 ppmw, within a factor of 2–3. This is based on 1) measured concentrations of noncrustal Mn in both snow and atmospheric aerosol at Barrow (Rahn and McCaffrey, 1979; Weiss *et al.*, 1978); 2) the measured fraction of soot in aerosol over Sweden (Brosset, 1978); and 3) the assumption that soot and Mn, both being in the submicron fraction, are removed from air into snow with the same efficiency.

In the absence of data on the soot content of snow, another speculation can be made from the estimates of Seiler and Crutzen (1980). They estimate the total worldwide production of graphitic carbon to be between 0.7 and 1.7×10^{15} g year^{-1}, and that 20–30% of it becomes airborne. If we make the naive assumption that this is uniformly distributed over

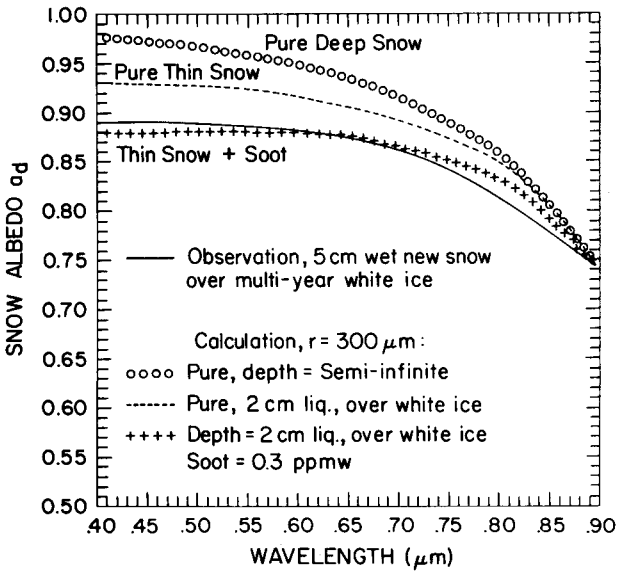

FIG. 8. Combined effect of finite depth and soot content on snow albedo a_d.

the earth's surface, the deposition rate would be 0.3 to 1.0 g m^{-2} $year^{-1}$. In the Arctic Ocean, where the mean annual precipitation is 13 g cm^{-2} $year^{-1}$, the carbon content would be 2–8 ppmw. This is 10–30 times as great as the amount of soot we think was present in the snow whose albedo was measured at T-3.

Even if the *general* level of soot in Arctic snow is insufficient to reduce the albedo, soot may still be the explanation of the low observed values at T-3. The measurements of Grenfell and Maykut (1977) were made within 500 m of the main camp on T-3, giving rise to the possibility of local pollution. The fuel which is burned for heating and electricity at Arctic and Antarctic camps typically releases 0.1–0.3% of its mass as soot particles (R. Charlson and J. Ogren, personal communication). Hanson (1980) noted that melt puddles on Arctic sea ice developed earliest in the camp areas, attributing this to soot contamination.

5. Combined effects of soot and finite depth on snow albedo

In Fig. 6 we used albedo calculations for a semi-infinite snowpack. However, one of the three snowpacks studied by Grenfell and Maykut (1977) was thin enough that we expect the underlying surface to influence the albedo. The middle solid line in Fig. 6 is for only 5 cm of wet new snow on top of multi-year white ice. We investigate the extent to which each of the two factors, finite depth and soot, can account for the reduction in albedo relative to that of pure deep snow. Both have the same qualitative effect, that of reducing the albedo only in the visible region.

Fig. 8 shows the wet new snow albedo measured by Grenfell and Maykut along with three model predictions. We assume the snow density was 0.4 g cm^{-2}, so that the snow depth was 2 cm liquid equivalent. The grain size is chosen as 300 μm to match the observed albedo at $\lambda = 0.9$ μm. The albedo of the underlying white ice we take as intermediate between curves *a* and *b* in Fig. 2 of Grenfell and Maykut (1977). This white ice has a maximum albedo of 0.84 at $\lambda = 0.4$ μm. The resulting albedo we calculate for the snow-ice system (without soot) is shown as the dashed line in Fig. 8. The albedo at $\lambda = 0.4$ μm is reduced by 4.4%, relative to semi-infinite snow. If the underlying surface had been perfectly black, the albedo would have been reduced by 8% instead of 4.4%.

The finite-depth effect thus can only partially account for the observed albedo. In order to reduce the calculated albedo to the observed levels we require the addition of 0.3 ppmw soot (plus signs in Fig. 8). Thus, to explain observations we need the same amount of soot whether we take into account the finite depth (Fig. 8) or not (Fig. 6c). This is because light does not penetrate as deeply in the dirty snow as it does in pure snow. Two centimeter liquid equivalent of soot-containing snow is actually effectively semi-infinite in this case, whereas the same depth of pure snow is not.

This effect can also explain the paradox described in Section 5e of Part I. In their study of the effect of snow depth, Giddings and LaChapelle (1961, Fig. 2) found the snow albedo at $\lambda = 0.59$ μm for grain size ~250 μm and $\mu_0 = 1$ to be within 3% of the asymptotic limit for a depth of 2 cm (~8 mm liquid equivalent). Fig. 13b in Part I shows that for pure snow about four times this depth would be required to reach within 3% of the semi-infinite albedo. The small 2 cm depth they observed corresponds to $\tau_0 \approx 120$ [Eq. (1) of Part I]. Our model for pure snow (Fig. 5b of Part I) would indicate that the semi-infinite limit when $(1 - \tilde{\omega}) = 4 \times 10^{-5}$ (corresponding in Fig. 3 of Part I to $\lambda = 0.59$ μm and $r = 250$ μm) is not attained until $\tau_0 \approx 300$, and that the asymptotic albedo is 95%, not the 75% measured by Giddings and LaChapelle. In order already at $\tau_0 = 120$ to reach an asymptotic albedo of 75%, $(1 - \tilde{\omega})$ would be required to be an order of magnitude larger, around 10^{-3} (Fig. 5b, Part I). This can be achieved if the observed sample (from Alta, Utah) contained ~1 ppmw of soot. This amount of soot would explain the low asymptotic albedo of 75%, as well as the much smaller depth required to reach this asymptote.

6. Snow albedo at Antarctic stations

Measurements of impurities in falling snow and in Antarctic ice cores show Antarctic snow to be ex-

ceptionally clean. Typical values of total insoluble impurities (0.01–0.03 ppmw) are far too small to have any effect on snow albedo.

The spectral albedo measurements of Liljequist (1956), plotted in Fig. 17 of Part I, do indeed show very high values in tolerable agreement with our calculations for pure snow (up to $a_d = 97\%$ at $\lambda = 0.5$ μm). However, recent measurements by Kuhn and Siogas (1978) showed albedo values at the South Pole to be only ~85–90% through the visible spectrum. These measurements are shown in Fig. 1 and were discussed in the Introduction, where it was pointed out that for shorter wavelengths our calculated albedos (circles in Fig. 1) significantly exceeded the observed ones. In order to reduce the calculated visible albedo (while retaining agreement with observation in the near IR) we require the presence of 1.5 ppmw of soot.[4] This is 50 to 100 times the concentration of *total* particulate matter observed in Antarctic ice cores, so this much soot cannot be naturally present in Antarctic snow. We think, however, that the particular snow sample examined here was contaminated by local pollution. The measurements were made ~1 km upwind from the South Pole station (Kuhn, personal communication). There is considerable soot released to the atmosphere here, both from aircraft exhaust in the summer and from furnaces and generators, especially in the winter. Also, in winter there are calm periods of strong surface temperature inversion during which the pollution dome extends in all directions, including the normal "upwind" direction. B. Parker and E. Zeller (personal communication), in the course of their chemical analyses of snow 2 km upwind from the South Pole, reported that all snow deposited since the establishment of the station during IGY (1957) contains visible filtrable carbon particles (radii ≥ 0.2 μm) but that snow below the 1957 level does not contain those particles. Our opinion is that albedos measured farther from the station would be higher (for $\lambda < 0.9$ μm) than those shown by the solid line in Fig. 1, and that they would approximate the circles plotted for pure snow in Fig. 1.

Because of the very uniform surface conditions across the Antarctic plateau, energy-budget calculations (e.g., Weller, 1980) generally make the assumption that measurements at stations are representative of large areas of the interior. We would therefore like to warn that the existence of local pollution at the larger stations can make their local radiation conditions uncharacteristic of the surrounding region.

[4] Kuhn (personal communication) calculates that his reported albedos should be adjusted upward by 4% (of their value) at all wavelengths due to the fact that the instrument box was in the field of view when the photometer head was facing downward. This means that we would require only 1 ppmw of soot to explain the measurement.

7. Summary

We have shown that the discrepancy between observations of visible snow albedo and calculations for pure snow (Fig. 17 of Part I) can be resolved if the snow whose albedo was measured was not pure. In order to match the observations of snow albedo at Station T-3 in the Arctic Ocean and at the South Pole Station, we require the presence of a grey impurity, i.e., one whose imaginary index of refraction varies little with wavelength. Graphitic carbon ("soot") has this property, and it is a normal component of the background atmospheric aerosol due to industrial sources as well as forest and brush fires. The snow at South Pole Station almost certainly suffers from local contamination and its albedo is unrepresentative of the rest of the Antarctic plateau where measured impurity concentrations are too low to affect the albedo.

Soot at T-3 in the Arctic Ocean, of which we require 0.3 ppmw to explain the albedo, may either be characteristic of the entire Arctic basin or derived from local (camp) pollution. This amount is not unrealistic if the soot which has been measured in Arctic air finds its way into the snow as well.

In middle latitudes the snow is closer to sources of dust and soot, but the snow accumulation rate is higher, so the concentration of impurities may not be larger until the snow begins to melt. The deposition rate of elemental carbon in Lake Michigan is now 30 μg cm^{-2} year^{-1} (J. Herring, U.S.G.S., unpublished manuscript). It was only half this value prior to 1900. The morphology of the particles indicates about one-half charcoal and one-half industrial sources. Assuming an annual precipitation of 1 m (liquid equivalent), the snow near Lake Michigan would contain 0.3 ppmw soot, the same as we need to explain albedo observations in the Arctic Ocean (Fig. 6), where the annual precipitation is only one-tenth that of Lake Michigan.

It is difficult to analyze for graphitic carbon, particularly because it must be distinguished from organic carbon. It has not been looked for in any of the many snow-chemistry studies in Antarctica and Greenland. Due to the excellent experimental work of Rosen and Novakov (1977, 1978), however, it has now become possible to identify and measure the carbonaceous content of aerosols. In order to test the predictions of our model, it will be necessary to make simultaneous measurements of snow spectral albedo, snow grain size, soot concentration and soot size distribution.

The snow samples reviewed here were from Arctic and Antarctic locations, and they exhibited "grey" albedo in the visible. In snowfields closer to desert areas and remote from population centers, such as the ice caps of the Tibetan Plateau, the principal absorptive component of the dust may be

iron oxide instead of carbon. The snow would then exhibit a peak in the spectral albedo near $\lambda = 0.6$ μm (Fig. 5), as has been seen by eye in Europe and New Zealand following dust storms in North Africa and Australia.

If the albedo of natural snow is being reduced by the presence of dust or soot, this could be an important climatic effect of tropospheric aerosols. Landsberg (1970) speculated that the climatic effects of aerosols in snow would be greater than their effects in the troposphere. Aerosols in the troposphere have competing effects on the radiation budget, in that they both absorb and reflect solar radiation, and emit infrared radiation. Carlson and Benjamin (1980) show that, for typical Saharan dust over the Atlantic, these effects roughly cancel each other for the top-of-atmosphere net flux. But when absorbing aerosols fall into snow, they have only one effect—that of reducing the shortwave albedo. The emissivity of snow in the infrared window region (8–12 μm) is very close to 1.0 (Figs. 8b and 11b of Part I) and the addition of parts-per-million amounts of dust does not change it.

In closing, we might note that *gross* amounts of carbon particles have in the past been suggested as effective melters of sea ice or modifiers of weather (Gray *et al.*, 1976). The present work indicates that such particles may have been having a climatic effect, albeit on a more subtle scale, over long periods of earth's history, which effect has been accentuated by man's industrial pollution.

Note added in proof. Grenfell *et al.* (1980) have recently collaborated to make simultaneous measurements of snow spectral albedo and soot content. Their measured grain sizes apparently are not the same as our effective spherical radii, so we deduce the effective optical grain size from the near-IR albedo measurements. It then appears that, in order to explain the visible albedos, we would need 2–5 times as much soot as was actually found in the snow. A factor of 2 difference in soot concentration can be explained by our use of graphite density instead of soot density (see footnote 3), but the remaining discrepancies remain to be investigated.

Acknowledgments. We thank Craig Bohren for first suggesting to us the importance of trace impurities in lowering snow albedo; Thomas Grenfell and Michael Kuhn for providing details of their experiments; and Robert Charlson, Peter MacKinnon, Kenneth Rahn, Hal Rosen, Lonnie Thompson and Ellen Mosley-Thompson for helpful discussion.

REFERENCES

Becquerel, J., and J. Rossignol, 1929: Spectral absorption of light and heat by pure inorganic substances and miscellaneous materials (nonmetals). *International Critical Tables*, Vol. 5, McGraw-Hill, 268–271.

Bergstrom, R. W., 1979: The effect of carbon particles on atmospheric radiation. *Carbonaceous Particles in the Atmosphere*, Lawrence Berkeley Laboratory, Publ. LBL-9037, 245–246.

Boutron, C., and C. Lorius, 1979: Trace metals in Antarctic snows since 1914. *Nature*, **277**, 551–554.

Brosset, C., 1978: Water-soluble sulphur compounds in aerosols. *Atmos. Environ.*, **12**, 25–38.

Byers, H. R., 1936: Meteorological history of the brown snowfall of February 1936. *Mon. Wea. Rev.*, **64**, 86–87.

Carlson, T. N., and S. G. Benjamin, 1980: Radiative heating rates for Saharan dust. *J. Atmos. Sci.*, **37**, 193–213.

Dalzell, W. H., and A. F. Sarofim, 1969: Optical constants of soot and their application to heat-flux calculations. *J. Heat Transfer*, **91**, 100–104.

Darby, D. A., L. H. Burckle and D. L. Clark, 1974: Airborne dust on the arctic pack ice, its composition and fallout rate. *Earth Planet. Sci. Lett.*, **24**, 166–172.

Dirmhirn, I., 1960: Starke Absorptionsschichten auf den Schneeoberflächen der Alpengletscher. *Wetter und Leben*, **12**, 152–153.

Dunne, T., and A. G. Price, 1975: Estimating daily net radiation over a snowpack. *Clim. Bull.*, McGill University, No. 18, 40–50.

Elgmork, K., A. Hagen and A. Langeland, 1973: Polluted snow in southern Norway during the winters 1968–1971. *Environ. Pollut.*, **4**, 41–52.

Falconer, R. E., and A. W. Hogan, 1971: Capture of aerosol particles by ice crystals. *Proc. Eastern Snow Conf., 1971*, Fredericton, N.B., 1–8.

Fischer, K., and G. Hänel, 1972: Bestimmung physikalischer Eigenschaftern atmosphärischer aerosolteilchen über dem Atlantik. *Meteor. Forschungsergeb.*, Reihe B, **8**, 59–62.

Foster, P. J., and C. R. Howarth, 1968: Optical constants of carbons and coals in the infrared. *Carbon*, **6**, 719–729.

Franklin, Rosalind E., 1950: The structure of carbon. *J. Chim. Phys.*, **47**, 573–575.

——, 1951: The structure of graphitic carbons. *Acta Cryst.*, **4**, 253–261.

Giddings, J. C., and E. R. LaChapelle, 1961: Diffusion theory applied to radiant energy distribution and albedo of snow. *J. Geophys. Res.*, **66**, 181–189.

Gillespie, J. B., S. G. Jennings and J. D. Lindberg, 1978: Use of an average complex refractive index in atmospheric propagation calculations. *Appl. Opt.*, **17**, 989–991.

Glazovskaya, M. A., 1954: Eolian deposits on Tien Shan glaciers (in Russian). *Priroda*, **43**, 90–92.

Gray, W. M., W. M. Frank, M. L. Corrin and C. A. Stokes, 1976: Weather modification by carbon dust absorption of solar energy. *J. Appl. Meteor.*, **15**, 355–386.

Greenaway, D. L., G. Harbeke, F. Bassani and E. Tosatti, 1969: Anisotropy of the optical constants and the band structure of graphite. *Phys. Rev.*, **178**, 1340–1348.

Grenfell, T. C., and G. A. Maykut, 1977: The optical properties of snow and ice in the Arctic basin. *J. Glaciol.*, **18**, 445–463.

——, D. K. Perovich and J. A. Ogren, 1980: Spectral albedos of an Alpine snowpack. *Cold Regions Sci. Tech.* (in press).

Haeberli, W., 1977: Sahara dust in the Alps—A short review. *Z. Gletscher. Glazialgeol.*, **13**, 206–208.

Hamilton, W. L., and C. C. Langway, Jr., 1967: A correlation of microparticle concentrations with oxygen isotope ratios in 700-year old Greenland ice. *Earth. Plan. Sci. Lett.*, **3**, 363–366.

Hammer, C. U., 1977: Dating of Greenland ice cores by microparticle concentration analyses. *Isotopes and Impurities in Snow and Ice*, IAHS Publ. No. 118, 297–301.

Hanson, A. M., 1980: The snow cover of sea ice during the Arctic ice dynamics joint experiment, 1975 to 1976. *Arctic Alpine Res.*, **12**, 215–226.

Hanson, K. J., 1960: Radiation measurement on the Antarctic

snowfield, a preliminary report. *J. Geophys. Res.*, **65**, 935–946.

Herron, M. M., C. C. Langway, Jr., H. V. Weiss and J. H. Cragin, 1977: Atmospheric trace metals and sulfate in the Greenland ice sheet. *Geochim. Cosmochim. Acta*, **41**, 915–920.

Higuchi, K., and A. Nagoshi, 1977: Effect of particulate matter in surface snow layers on the albedo of perennial snow patches. *Isotopes and Impurities in Snow and Ice*, IAHS Publ. No. 118, 95–97.

Khromov, S., 1931: Yellow snow (in Russian). *Mirovendenie*, **20**, 106–107.

Koerner, R. M., 1977: Distribution of microparticles in a 299 m core through the Devon Island ice cap, Northwest Territories, Canada. *Isotopes and Impurities in Snow and Ice*, IAHS Publ. No. 118, 371–376.

Kohno, S., and N. Maeno, 1979: Migration of solid particles in melting snow. *Low Temp. Sci.*, **A38**, 81–92.

Kuhn, M., and L. Siogas, 1978: Spectroscopic studies at McMurdo, South Pole and Siple Stations during the austral summer 1977–78. *Antarctic J. U.S.*, **13**, 178–179.

Kumai, M., 1976: Identification of nuclei and concentrations of chemical species in snow crystals sampled at the South Pole. *J. Atmos. Sci.*, **33**, 833–841.

——, 1977: Electron microscope analysis of aerosols in snow and deep ice cores from Greenland. *Isotopes and Impurities in Snow and Ice*. IAHS Publ. No. 118, 341–350.

Landsberg, H. E., 1970: Man-made climatic changes. *Science*, **170**, 1265–1274.

Langway, C. C., Jr., G. A. Klouda, M. M. Herron and J. H. Cragin, 1977: Seasonal variations of chemical constituents in annual layers of Greenland deep ice deposits. *Isotopes and Impurities in Snow and Ice*, IAHS Publ. No. 118, 302–306.

Liljequist, G. H., 1956: Energy exchange of an Antarctic snowfield. Short-wave radiation (Maudheim, 71°03′S, 10°56′W). *Norwegian-British-Swedish Antarctic Expedition, 1949–52, Scientific Results*, Vol. 2, Part 1A, Norsk Polarinstitutt, 107 pp.

Lindberg, J. D., 1975: The composition and optical absorption coefficient of atmospheric particulate matter. *Opt. Quant. Electron.*, **7**(Review), 131–139.

Magono, C., T. Endoh, F. Ueno, S. Kubota and M. Itasaka, 1979: Direct observations of aerosols attached to falling snow crystals. *Tellus*, **31**, 102–114.

Marshall, P., and E. Kidson, 1929: The dust-storm of October 1928. *N.Z. J. Sci. Tech.*, **10**, 291–299.

McCartney, J. T., J. B. Yasinsky and S. Ergun, 1965: Optical constants of coals by reflectance measurements in the ultraviolet and visible spectrum. *Fuel*, **44**, 349–354.

Mita, A., and K. Isono, 1980: Effective complex refractive index of atmospheric aerosols containing absorbing substances. *J. Meteor. Soc. Japan*, **58**, 69–80.

Mullen, R. E., D. A. Darby and D. L. Clark, 1972: Significance of atmospheric dust and ice rafting for Arctic Ocean sediment. *Geol. Soc. Amer. Bull.*, **83**, 205–212.

Murozumi, M., T. J. Chow and C. Patterson, 1969: Chemical concentrations of pollutant lead aerosols, terrestrial dusts and sea salts in Greenland and Antarctic snow strata. *Geochim. Cosmochim. Acta*, **33**, 1247–1294.

Oeschger, H., U. Schotterer, B. Stauffer, W. Haeberli and H. Röthlisberger, 1977: First results from alpine core drilling projects. *Z. Gletscher. Glazialgeol.*, **13**, 193–204.

Patterson, E. M., and D. A. Gillette, 1977: Commonalities in measured size distributions for aerosols having a soil-derived component. *J. Geophys. Res.*, **82**, 2074–2082.

——, D. A. Gillette and B. H. Stockton, 1977: Complex index of refraction between 300 and 700 nm for Saharan aerosols. *J. Geophys. Res.*, **82**, 3153–3160.

Peterson, C. M., H. J. Paulus and G. H. Foley, 1969: The number-size distribution of atmospheric particles during temperature inversions. *J. Air Pollut. Control Assoc.*, **19**, 795–801.

Pollack, J. B., O. B. Toon and B. N. Khare, 1973: Optical properties of some terrestrial rocks and glasses. *Icarus*, **19**, 372–389.

Post, A., and E. R. LaChapelle, 1971: *Glacier Ice*. University of Washington Press, 110 pp.

Prospero, J. M., 1979: Mineral and sea salt aerosol concentrations in various ocean regions. *J. Geophys. Res.*, **84**, 725–731.

Pruppacher, H. R., and J. D. Klett, 1978: *Microphysics of Clouds and Precipitation*. Reidel, 714 pp.

Rahn, K. A., and R. J. McCaffrey, 1979: Compositional differences between Arctic aerosol and snow. *Nature*, **280**, 479–480.

Robinson, W. O., 1936: Composition and origin of dust in the fall of brown snow, New Hampshire and Vermont, February 24, 1936. *Mon. Wea. Rev.*, **64**, 86.

Rosen, H., and T. Novakov, 1977: Raman scattering and the characterization of atmospheric aerosol particles. *Nature*, **266**, 708–710.

——, and ——, 1978: Identification of primary particulate carbon and sulfate species by Raman spectroscopy. *Atmos. Environ.*, **12**, 923–927.

——, A. D. A. Hansen, L. Gundel and T. Novakov, 1978: Identification of the optically absorbing component in urban aerosols. *Appl. Opt.*, **17**, 3859–3861.

Seiler, W., and P. J. Crutzen, 1980: Estimates of gross and net fluxes of carbon between the biosphere and the atmosphere from biomass burning. *Climatic Change*, **2**, 207–247.

Stephenson, P. J., 1967: Some considerations of snow metamorphism in the Antarctic ice sheet in the light of ice crystal studies. *Physics of Snow and Ice, Proceedings of the International Conference on Low Temperature Sciences*, H. Ōura, Ed., 14–19 August 1966, Sapporo, Japan, Bunyeido Printing Company, 725–740.

Thompson, L. G., 1977: Variations in microparticle concentration, size distribution and elemental composition found in Camp Century, Greenland, and Byrd Station, Antarctica, deep ice cores. *Isotopes and Impurities in Snow and Ice*, IAHS Publ. No. 118, 351–364.

——, S. Hastenrath and B. Morales-Arnao, 1979: Climatic ice core records from the tropical Quelccaya Ice Cap. *Science*, **203**, 1240–1243.

Toon, O. B., J. B. Pollack and B. N. Khare, 1976: The optical constants of several atmospheric aerosol species: Ammonium sulfate, aluminum oxide and sodium chloride. *J. Geophys. Res.*, **81**, 5733–5748.

Twitty, J. T., and J. A. Weinman, 1971: Radiative properties of carbonaceous aerosols. *J. Appl. Meteor.*, **10**, 725–731.

Weiss, H. V., M. M. Herron and C. C. Langway, Jr., 1978: Natural enrichment of elements in snow. *Nature*, **274**, 352–353.

Weiss, R. E., A. P. Waggoner, R. Charlson, D. L. Thorsell, J. S. Hall and L. A. Riley, 1979: Studies of the optical physical and chemical properties of light absorbing aerosols. *Carbonaceous Particles in the Atmosphere*, Lawrence Berkeley Laboratory, Publ. LBL-9037, 257–262.

Weller, G. E., 1980: Spatial and temporal variations in the south polar surface energy balance. *Mon. Wea. Rev.*, **108**, 2006–2014.

Whitby, K. T., 1979: Size distribution and physical properties of combustion aerosols. *Carbonaceous Particles in the Atmosphere*, Lawrence Berkeley Laboratory, Publ. LBL-9037, 201–208.

Windom, H. L., 1969: Atmospheric dust records in permanent snowfields: Implications to marine sedimentation. *Geol. Soc. Amer. Bull.*, **80**, 761–782.

Wiscombe, W. J., and S. G. Warren, 1980: A model for the spectral albedo of snow. I. Pure snow. *J. Atmos. Sci.*, **37**, 2712–2733.